

Chapter 2

Background

2.1 The Heart and the Circulatory System

In mammals, the circulatory system has two components: the pulmonary circuit, whose function is to oxygenate the blood via the lungs, and the systemic circuit, whose function is to provide oxygenated and nutrient rich blood to the cells around the body. To drive these two systems, the heart can be thought of as being two pumps in series, split between the left and the right. The right side drives the pulmonary circuit and the left side drives the systemic circuit, as shown in Fig. 2.1. The arterial system is a network of blood vessels which carry blood away from the heart. The venous system is a network of blood vessels which carry blood towards the heart. Capillaries are vessels with very thin walls through which nutrients and oxygen can permeate into the surrounding cells. They link the arterial and venous systems outside the heart.

2.1.1 Gross Anatomy of the Heart

Each of the two pumps in the heart contains two chambers: an atrium and a ventricle [1] (Fig. 2.2). The atria collect blood from the venous system and pump it into the ventricles. The ventricles pump blood through the arterial and venous systems of the pulmonary and systemic circuits. The atria are superior to the ventricles, and lie to the right side in the human body (Fig. 1.1). Separating the two atria is the inter-atrial septum (AS), and the inter-ventricular septum (IVS) separates the two ventricles. The walls of the atria and ventricles are separated by a layer of connective tissue which contains substantial amounts of fat. This provides an electrical insulation between the walls of the different chambers. Between the chamber cavities of the atria and ventricles are the tricuspid valve (right) and the bicuspid valve (left) which are extensions of this fatty connective tissue. These prevent backflow of blood from the ventricles into the atria.

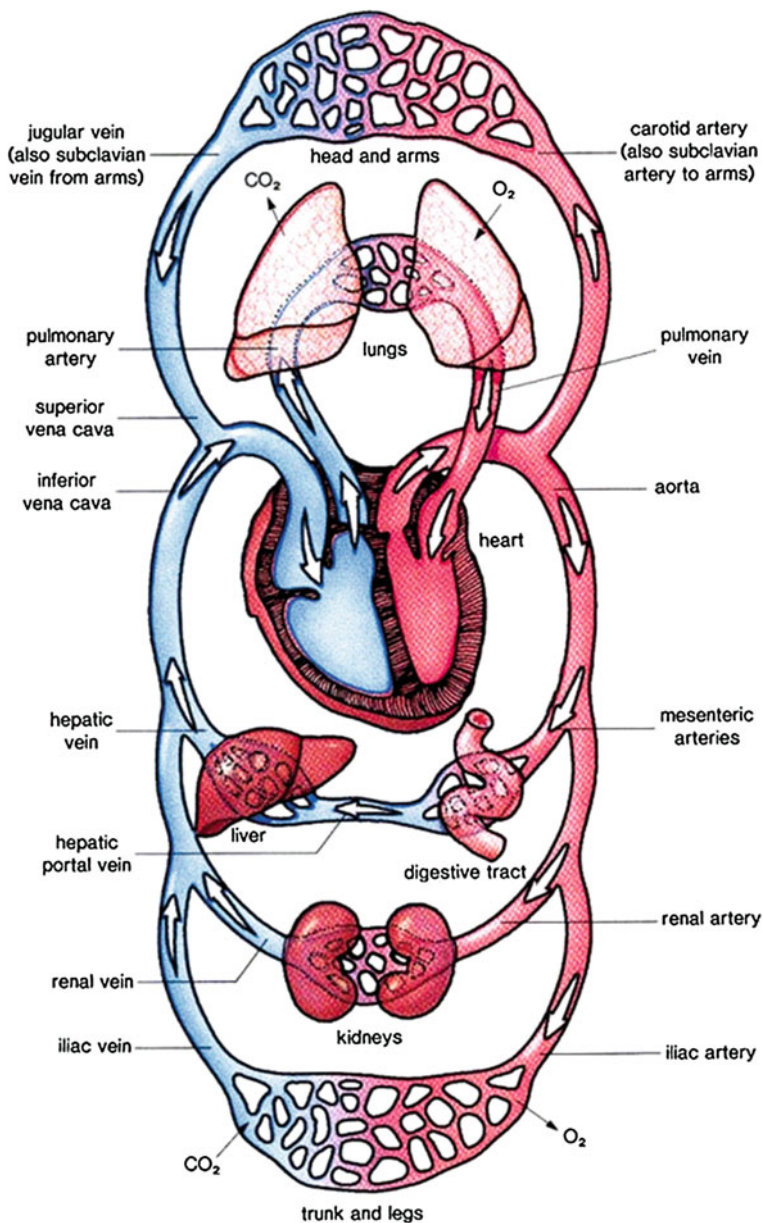
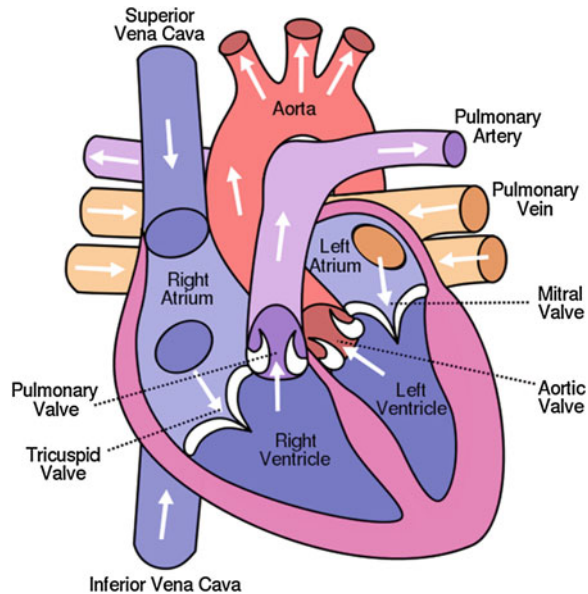


Fig. 2.1 Schematic of the circulatory system. Schematic of the components of the circulatory system. Oxygenated blood is shown in *right* and deoxygenated blood in *left*. With the exception of the pulmonary circuit, blood vessels on the left of the page are part of the venous system and those on the right are part of the arterial system. The capillaries are the network like structures which join the arterial and venous systems outside the heart. Adapted from [2]

Fig. 2.2 Gross anatomy of and blood flow within the heart. Schematic of the structure of the heart and the primary blood vessels. Arrows indicate the direction of blood flow in each region. Adapted from [3]



The size and structure of the atria and ventricles are linked to their respective functions. The pressures the atria need to develop to pump the blood through the valves into the ventricles are relatively low compared to that of the ventricles, which need develop much greater pressures to pump blood around the circulatory systems. For this reason, the atria are relatively small and contain only thin walls, whereas the ventricles are much larger (2–5 times) and contain thick walls [1]. The left ventricle (LV) is also noticeably larger than the right ventricle (RV), as it must develop a greater pressure to force blood through the much larger systemic circulatory system. Such an asymmetry between left and right is not mirrored in the atria.

2.1.2 Blood Flow Through the Heart

A schematic of the blood flow in the heart is shown in Fig. 2.2. As the blood returns from the systemic circuit, it enters the right atrium (RA) through the superior and inferior vena cava (SVC and IVC, respectively). These are the major veins into which all systemic veins eventually connect. From here, it is pumped through the tricuspid valve into the right ventricle. The valve then shuts as the ventricle begins to contract, preventing backflow into the atria. During right ventricular contraction, blood is forced through the pulmonary valve into the pulmonary artery. This valve then also closes to prevent backflow into the ventricles. Successive beats then force the blood through the pulmonary system and

into the lungs, where it is oxygenated. From here, it returns to the heart through the pulmonary veins and into the left atrium, where it is then pumped through the mitral valve into the left ventricle, in a similar manner as in the right side. From the left ventricle it is forced through the aortic valve into the aorta. The aorta is the primary artery of the body, and successively splits to form smaller and smaller arteries and capillaries which are responsible for delivering oxygenated blood throughout the body. It is important to note that the heart itself must receive some of this blood through capillaries in the walls, as it cannot (in general) receive oxygen from the blood within its chambers. This is through the coronary circulatory system. From here, blood returns to the heart through the coronary sinus, and the cycle repeats. The time during which the heart is contracting is known as systole. After the systolic period, the heart must relax for some time to allow it to refill with blood. This relaxation time is known as diastole.

2.1.3 Detailed Anatomy of the Atria

The focus of this thesis is on human atrial modelling and hence it is necessary to describe the anatomy of the atria in more detail. Both the right and left atrium are thin walled and contain an area which is greatly expandable when it is filled with blood. This area is known as the atrial appendage, and becomes a flaccid, wrinkled flap when it is not filled with blood. It is also known as the auricle, because it reminded early anatomists of the outer ear [1]. The SVC opens into the posterior, superior RA and carries all blood returning from the head, neck, chest and upper limbs. The IVC opens into the posterior, inferior RA and carries blood returning from the rest of the body, including the lower limbs. Blood from the coronary circulatory system returns to the right atrium through the coronary sinus (CS). The CS is a large, thin walled vein which opens into the RA inferior to the SVC in the posterior AS. The AS is a thick muscular structure which separates the two atria. Also present in the AS is the fossa ovalis. This is a small, shallow, oval depression which is a remnant of the embryonic foramen ovale, a hole between the right and left atria which permitted blood flow from the right atrium directly into the left in foetuses before the lungs have fully developed. In the healthy human heart this hole has closed to become the fossa ovalis within three months of birth.

The posterior wall of the RA and the AS are smooth, whereas the right atrial appendage (RAA) contains prominent muscular ridges called the pectinate muscles (PM). The PMs contain a high degree of fibre organisation and are a part of the cardiac conduction system (Sect. 2.1.4). The PMs connect to another large muscular ridge which extends from the SVC to the IVC, with the RAA and the PMs to one side and the AS to the other side. This is the crista terminalis (CT), and it too contains a highly organised fibrous structure. At the superior of the CT is Bachmann's bundle (BB), which extends from the CT near the SVC deep into the LA, although the exact extent of the BB can vary considerably between subjects [4]. The LA is largely similar to the RA, with a few notable differences. The

pulmonary veins (PV), returning blood from the lungs, enter the LA via four trunks, two on the left and two on the right. There is no CT in the left atrium, and the PMs are less distinct.

The sino-atrial node (SAN), known as the cardiac pacemaker, drives the electrical activity of the heart in healthy subjects. It is situated posterior to the CT, near the SVC high in the RA. Originally thought to be small and node like, it is now known to be an extensive structure which can stretch from the SVC to the IVC [5–8]. It is heterogeneous in that the cells in the periphery have different properties to those in the centre [9–11]. The atrioventricular node (AVN) is the secondary pacemaker of the heart and also represents the only electrical connection between the atria and the ventricles. It lies in the AS, near the CS and superior to the IVC. It is also a heterogeneous structure, made up of three main components: the fast pathway, the slow pathway and the penetrating bundle. It is the penetrating bundle in which the electrical connection to the ventricles is located. The penetrating bundle is insulated from the surrounding atria and hence electrical activity can only reach it through either of the two pathways [12].

2.1.4 The Cardiac Conduction System and the Heartbeat

Cardiac myocytes (the muscle cells within the heart) are electrically excitable. It is this electrical excitation which is related to the contractile function of the heart. The spread of electrical activity throughout the myocardium is responsible for the coordinated contraction which allows the heart to drive the circulatory systems.

The cardiac conduction system (CCS) is a specialised network of cardiac myocytes whose main function is to initiate and conduct the electrical activity throughout the heart. Its function has strong implications for cardiac output, and many cardiac diseases result from dysfunction of the CCS. A simplified schematic of the CCS is shown in Fig. 2.3. Excitation is initiated in the RA from the centre of the SAN. Myocytes within the SAN are able to spontaneously generate electrical excitation at rates of between 60 and 100 bpm [1, 13]. Mechanisms by which they are able to do so are discussed in Sect. 2.3.5. From the SAN, excitation is rapidly conducted along the bundles of the CT and PM through the RA, and via BB into the LA. The existence of internodal pathways in the right atrium is disputed, although recent micro-CT evidence in the rabbit atria suggest they are present [14]. Their function would be to rapidly conduct electrical excitation to the AVN. Myocytes within the AVN are also able to spontaneously generate electrical excitation, at rates slower than that of the SAN (20–40 bpm). Excitation travels through the fast and slow pathways of the AVN and into the penetrating bundle. Total conduction through the AVN takes about 100 ms. This delay is important to allow the atria to contract and force blood into the ventricles, before ventricular contraction begins. This is the primary reason that the AVN is the only electrical connection between the atria and ventricles in the healthy heart: if they were not insulated, this delay would not be possible. Connected to the penetrating bundle is

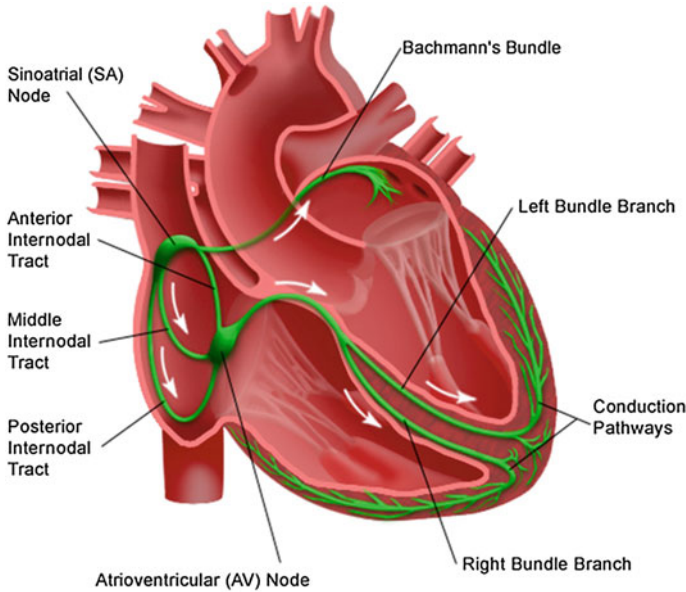


Fig. 2.3 The cardiac conduction system. Schematic of the cardiac conduction system, shown in *green*. Labelled are the SAN, AVN, BB and the Purkinje network (*right* and *left* bundle branches). Adapted from [15]

the His-Purkinje network. This is a vast network of rapidly conducting myocytes which spread out around the endocardial surface of the ventricles. The Purkinje network is essentially a fractal pattern similar in structure to that of the arterial and capillary system. It first splits into two main branches, the right and left branch, for each ventricle, and then successively bifurcates into smaller and smaller networks. The extent and number of vertices of the network can vary considerably from person to person. The Purkinje network is largely insulated from the ventricles, and only forms electrical connections at sites known as insertion points. The role of the Purkinje network is to rapidly spread excitation around the ventricles such that they contract in a coordinated manner. In human, it takes around only 75 ms for the Purkinje network to conduct the electrical excitation around the entire ventricles.

2.2 The Cardiac Myocyte

Cardiac myocytes, or cardiomyocytes, are the muscle cells which occupy the majority of the myocardial mass. They contain a network of fibres, comprised of a highly organised cross striated distribution of two filaments: the thick filament comprised largely of myosin polymers and titin, and the thin filament comprised of

double stranded actin polymers including tropomyosin and the troponin complex [16]. They contain just a single nucleus, as opposed to skeletal muscle cells which contain many. The fluid in the intracellular space of the myocyte is known as the cytosol. Cardiomyocytes are connected through intercalated discs, which form a strong mechanical and electrical connection between adjacent cells. Cardiomyocytes vary in size and shape depending on the region from which they are attained. In human, they are typically cylindrical and between 50 to 150 μm long with a radius of 10–20 μm . They are grouped by shape and function: those of the working myocardium (WM), whose main function it is to contract and are found in the walls of the atria and ventricles, and specialised cells of the CCS. The myocytes of the WM have far more contractile elements than those of the specialised CCS [16]. Surrounding each myocyte is the plasma membrane, or the sarcolemma. This is impermeable to ions except through specific structures (Sect. 2.3.1). Within the myocyte is a second membrane structure called the sarcoplasmic reticulum. This acts as a Ca^{2+} store and has important implications for Ca^{2+} dynamics and contraction (Sect. 2.3.4).

2.3 Cardiac Electrophysiology

Cardiac electrophysiology refers to the description of the electrophysiological properties of cardiac myocytes. For the purposes of this thesis, this pertains to the flow of ions into and out of the cell, the cycle of ions within the cell and the mechanisms by which these processes occur.

2.3.1 The Cell Membrane

The cell membrane, or sacolemma, is a thin phospholipid bilayer composed of different proteins which separate the intracellular and extracellular spaces (Fig. 2.4). These proteins contain a hydrophilic head, which interacts with the fluids on either side of the membrane, and a hydrophobic tail. The difference of charge in the intracellular and extracellular spaces results in a potential difference across the cell membrane. This is referred to as the transmembrane potential and denoted V_m . By convention, the transmembrane potential is defined as the difference between the internal and external potentials, as such:

$$V_m = u_i - u_e \quad (2.1)$$

where u is the potential, i is intracellular and e is extracellular.

Within the phospholipid bilayer structure are found many different proteins. Integral proteins lie across it and peripheral proteins on either side, interacting with the fluids in the intracellular and extracellular spaces. Ions can only flow into and

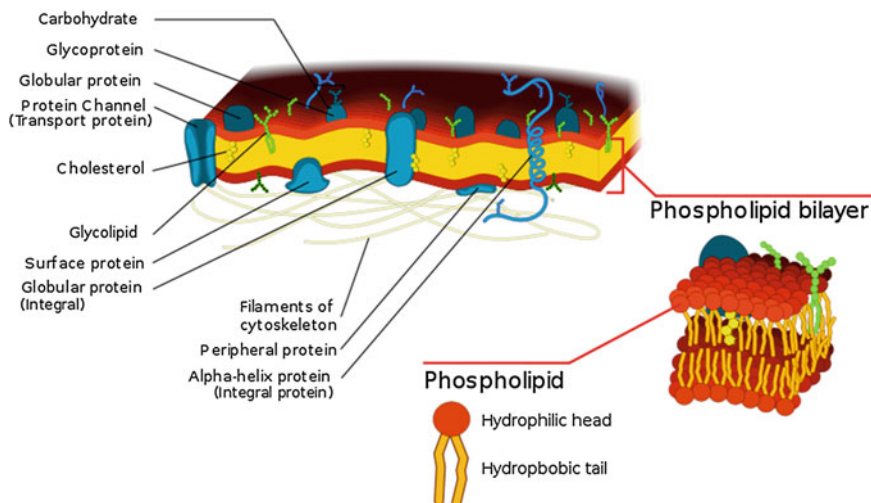


Fig. 2.4 Plasma membrane. Schematic of the cell membrane, or sarcolemma. Illustrated is the phospholipid bilayer and some of the proteins present. Adapted from [17]

out of the cell through specialised integral protein structures. It is these structures which are responsible for the excitability of cardiomyocytes. There are primarily three different types of structure through which ions can flow, relevant to this thesis: Ion channels, Ion exchangers and Ionic pumps. All have ion selectivity: they are permeable to only one or two types of ions. Ion channels are generally permeable to just one type of ion whereas Ion exchangers are permeable to two. The most abundant in cardiomyocytes are ion channels. Ion channels permit passive processes, that is, they exert no force on or supply no energy to the ions themselves. When a channel opens, the ions flow according to their electrochemical gradient. The opening and closing of the channel is a result of conformational changes in the folding of the protein.

Ion channels may have both activation and inactivation processes, referred to as gates [18]. The state of these gates determines whether or not a current can flow through the channel. It is simplest to describe these processes schematically, and a simplified illustration of an ion channel which contains both activation and inactivation gates is shown in Fig. 2.5. The channel shown has an electrochemical gradient towards the intracellular space, and hence the net flow of ions would be into the cell. Panel A shows the channel in a state in which it is neither activated nor inactivated. This may correspond to the resting state of a channel. The activation gate (blue) is not activated and hence is closed. The inactivation gate (red) is not inactivated and hence is not closed. In panel B, the activation gate is now activated and has opened. The inactivation gate is still not inactivated, and hence the channel itself is open. This is the only state in which current can flow. In panel C, the activation gate is still open but now inactivation has occurred and the inactivation gate has closed. This prevents flow of a current, and the channel is

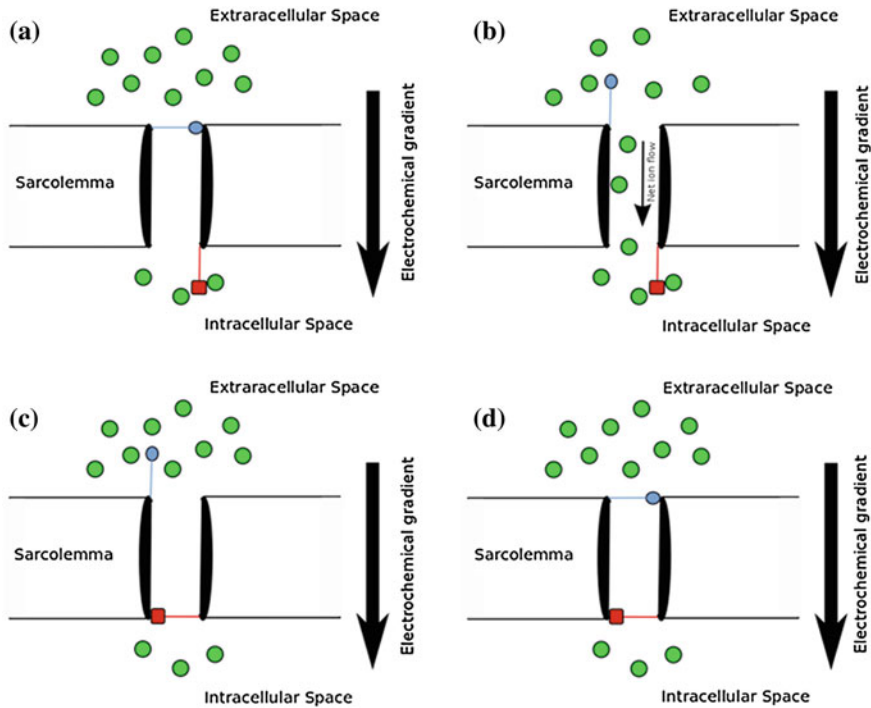


Fig. 2.5 Ion channel schematic. A simplified schematic of an ion channel which possesses both activation and inactivation gates, in 4 different states. The ions to which the channel is permeable are shown as *green circles*. The activation gate is in *blue circle* and the inactivation gate is in *red (square)*. **a** The channel is not activated or inactivated. **b** The channel is activated but not inactivated. **c** The channel is activated and inactivated. **d** The channel is not activated, but is inactivated. It can be seen that only in state **b** can a current flow (color figure online)

closed. In panel D, the activation gate is now closed (a process referred to as deactivation) and the inactivation gate is still inactivated. The process of inactivation has important implications for current flow: if a channel is inactivated, current cannot flow regardless of whether the activation gate is open or closed. This results in behaviour such as recovery time from inactivation. The control of activation and inactivation can occur primarily through either dependence on V_m (voltage gated channels), the presence or absence of ions or structures (ligand gated channels), the level of acidity (pH gated channels) or the physical state of the membrane (mechanically gated channels). Voltage gated channels are the most relevant to the contraction of a cardiomyocytes, though it is worth noting that both ligand gated and mechanically gated channels have been characterised in relation to the cardiac action potential.

As opposed to ion channels, ionic pumps permit active processes: they require energy from ATP. They can, therefore, move ions against their electrochemical gradient. Ion exchangers cannot be classified as either passive or active: they are

co-transporters, and use the energy of one ion flowing with its electrochemical gradient to move another against it. Both pumps and exchangers are especially important in preventing ion concentration build up or depletion in the intracellular space and hence play a role in the cyclic ability of a cell to be repeatedly excited.

2.3.2 Sarcolemmal Ion Channel Currents

The primary ions involved in the ion channels, pumps and exchangers in cardiac myocytes are sodium (Na^+), potassium (K^+) and calcium (Ca^{2+}). Chloride ions (Cl^-) are also involved, to a lesser extent. An inward current is defined as one in which positive ions flow into the cell. This acts to raise the transmembrane potential. An outward current lowers the potential. Ion channels permeable to sodium and calcium result in inward currents in physiological voltage ranges for cardiomyocytes. Ion channels permeable to potassium ions carry outward currents. There can be many different types of channel or process permeable to each ion. These are grouped by common kinetics and properties. Each type of channel carries an associated current. Because there are many of each type of channel in the membrane, the current is that of the net flow of ions through all of that type of channel. The way in which each current interacts is discussed in the next section. Table 2.1 summarises the main currents involved in cardiomyocytes.

The ion channels themselves are complex proteins which contain a folded unique sequence of amino acids, defined by the sequence of a gene. The channel proteins are grouped into families, responsible for each current. The particular protein within each family primarily responsible for the encoding of an ion channel can differ between species. Messenger RNA (mRNA) is linked to the

Table 2.1 Primary sarcolemmal ion currents in cardiac myocytes

Symbol	Name	Type	Permeability
I_{Na}	Fast acting sodium current	Ion channel	Na^+
$I_{\text{Na,L}}$	Late acting sodium current	Ion channel	Na^+
$I_{\text{Ca,L}}$	L-type calcium current	Ion channel	Ca^{2+}
$I_{\text{Ca,T}}$	T-type calcium current	Ion channel	Ca^{2+}
I_{to}	Transient outward current	Ion channel	K^+
I_{Kur}	Ultra-rapid potassium current	Ion channel	K^+
I_{Kr}	Rapid delayed rectifying K^+ current	Ion channel	K^+
I_{Ks}	Slow delayed rectifying K^+ current	Ion channel	K^+
I_{K1}	Inwardly rectifying K^+ current	Ion channel	K^+
I_{KACh}	Acetylcholine activated K^+ current	Ion channel	K^+
I_{f}	Hyperpolarisation activated Funny current	Ion channel	Na^+/K^+
I_{NaCa}	Sodium Calcium exchanger current	Ion exchanger	$\text{Na}^+/\text{Ca}^{2+}$
I_{NaK}	Sodium potassium pump	Ionic pump	Na^+/K^+
I_{CaP}	Calcium pump	Ionic pump	Ca^{2+}

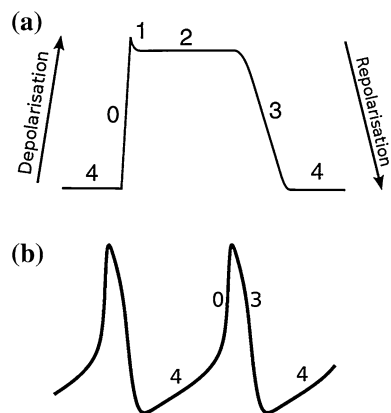
coding of the channel and hence mRNA levels can be indicative of channel expression.

2.3.3 The Cardiac Action Potential

The result of the action of the sarcolemmal ion currents is to cyclically change the transmembrane potential. This is known as the action potential (AP). Whereas there is a large degree of heterogeneity between the morphologies of the APs in different regions and species, they can none-the-less be described within the same framework. This consists of labelling distinct phases of the AP. Each phase corresponds to the action of one or more of the sarcolemmal ion currents. A labelled schematic of a cardiac action potential for a myocyte of the WM is shown in Fig. 2.6a.

The resting potential (RP) of the AP is the potential at which the membrane would remain if it were not perturbed. This is labelled as phase 4 and is negative, usually between -70 and -85 mV. Potentials in this range and more negative are referred to as hyperpolarised. The RP is largely determined by I_{K1} , I_{NaCa} and background currents [19]. A supra-threshold electrical stimulus applied to the myocyte then initiates a fast upstroke known as phase 0. This is called a depolarisation as its action is to make the transmembrane potential less negative. It is primarily a result of the fast influx of Na^+ ions carried by I_{Na} . I_{Na} then quickly inactivates, and the transient outward potassium current, I_{to} , becomes active causing a small negative deflection in the AP. This is known as phase 1 repolarisation (repolarisation because it acts to make the V_m more negative again) and is also referred to as the notch. Following this, I_{CaL} and other K^+ currents (e.g. I_{Ks} , I_{Kur}) all activate and this balance of inward and outward currents results in a plateau, corresponding to phase 2. After some time, I_{CaL} inactivates and the potassium currents act to fully repolarise the AP back to the RP. This is phase 3 or

Fig. 2.6 Phases of the action potential. **a** The phases of an action potential from the working myocardium. The numbers correspond to the phases referred to in the text. The direction of deflections known as depolarisations and repolarisations are indicated by the arrows. **b**. Phases of a spontaneously depolarising action potential. Not all phases are present in this form of action potential



terminal repolarisation. The negative RP deactivates the potassium channels and hence the AP is returned to the stable phase 4 until another stimulus is applied or received.

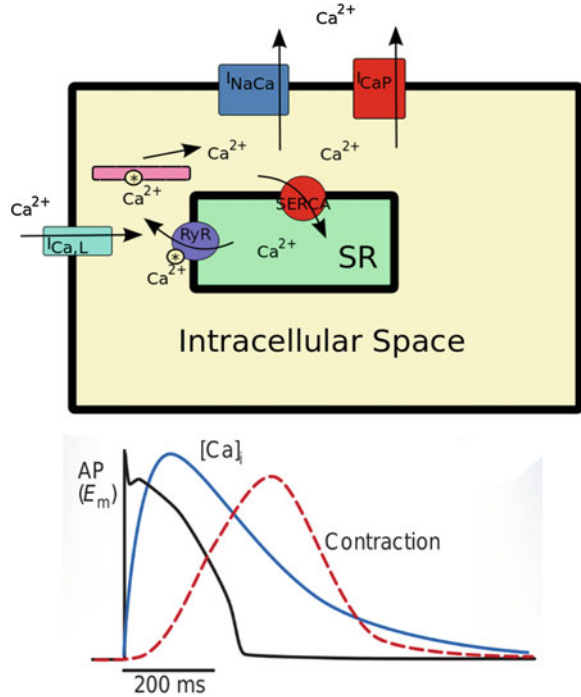
The large degree of electrophysiological heterogeneity observed in the heart manifests as different morphologies of the AP. These differences can take the form of different upstroke velocities during phase 0, the prominence of the notch in phase 1, the length and shape of the plateau in phase 2, the gradient of repolarisation in phase 3 and the RP itself in phase 4. Heterogeneities are a result of the differing relative magnitudes of each current with respect to the others. For example, a myocyte which has a higher expression of I_{CaL} is likely to have a more pronounced and longer plateau than a myocyte with a lower expression of I_{CaL} , and one with a greater expression of I_{K1} will have a more negative RP.

The morphology of the AP associated with the pacemaker myocytes which have the ability to spontaneously depolarise have some marked differences to that of the working myocardium (Fig. 2.6b). Never-the-less, they can still be described within the same framework. They tend not to reach as negative a potential as that of the WM, reaching the most negative in a region of -50 to -60 mV. This is partly due to a lower expression of I_{K1} but also due to the presence of the inward current I_f . Phase 4 of the AP is no longer stable and hence it has less meaning to denote it a ‘resting potential’. Instead, I_f and I_{CaT} act to slowly depolarise the potential (Sect. 2.3.5). The gradient of the upstroke during phase 0 is significantly shallower due to a lower expression of I_{Na} . They have a distinct lack of a phase 1 notch or flattening during the phase 2 plateau. Instead, phase 3 directly follows phase 0.

2.3.4 The Sarcoplasmic Reticulum, the CICR Cycle and the Ca^{2+} Transient

The sarcolemmal ion currents not only act to change the transmembrane potential but also the concentrations of the respective ions in the intracellular space. It is the presence of Ca^{2+} ions in the intracellular space which is related to the actual contraction of the myocyte. The sarcoplasmic reticulum (SR) plays an important role in the regulation of Ca^{2+} ions inside the cell. The membrane of the SR contains structures similar to those of the ion channels and pumps found in the sarcolemma. The ryanodine receptors (RyR) are analogous to a ligand gated ion channel. Ca^{2+} in the intracellular space binds with the receptors and this causes release of Ca^{2+} from the SR into the intracellular space [20]. They are located in close proximity to the L-type Ca^{2+} channels and it is the influx of Ca^{2+} ions due to I_{CaL} during phase 2 of the AP which causes this Ca^{2+} release. This process is known as Calcium-Induced-Calcium-Release (CICR) [20]. It is the Ca^{2+} released from the SR which binds with the contractile proteins, causing them to shorten and the cell to contract. Ca^{2+} is then released from its binding sites on these proteins

Fig. 2.7 The Ca^{2+} cycle and the Ca^{2+} transient. A vastly simplified schematic of the intracellular calcium cycle. Arrows indicate the net direction of the flow of Ca^{2+} ions. Ca^{2+} binding sites are indicated by an *asterisk*. The contractile element is shown as the *elongated rectangle* in the intracellular space. This element contains many different processes which are not shown in this figure. All processes referred to in the text are labelled in this figure. Below is a schematic example of the Ca^{2+} transient and resulting contraction associated with an AP. This is adapted from [20]



into the intracellular space. The SR Ca^{2+} pump regulated by SERCA then acts to pump Ca^{2+} back into the SR, restoring the concentration of Ca^{2+} ions within it. Ca^{2+} is also extruded from the intracellular space into the extracellular space via the sarcolemmal Ca^{2+} pump (I_{CaP}) and the sodium-calcium exchanger (I_{NaCa}). This cycle is illustrated in Fig. 2.7a. The cyclic change to the intracellular Ca^{2+} concentration is known as the calcium transient. A typical Ca^{2+} transient associated with an AP, and the tension development as a result is shown in Fig. 2.7b. Please note that this is a vastly simplified description of the Ca^{2+} cycle. The binding of calcium with the contractile elements, the other calcium buffers in the cytosol and the structure within the SR have not been described. For these, the reader is referred to [20].

2.3.5 Pacemaking Mechanisms

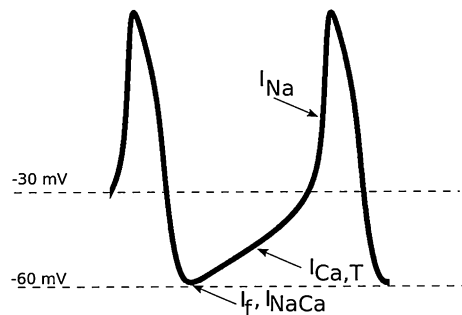
There is some debate as to the exact mechanisms which are dominantly responsible for the spontaneous depolarisation observed in pacemaker potentials. The mechanisms in question are the membrane clock and the calcium clock [21–23]. The membrane clock refers to the action of the sarcolemmal ion currents carried by I_f and I_{CaT} . I_f , so called the funny current because of its many unusual

properties, including its permeability to both Na^+ and K^+ ions, was first described by Noble's school in the late 1970s and early 1980s [22, 24–27]. It was through this work that DiFrancesco described the funny current as an inward current activated on hyperpolarisation, rather than an outward current deactivated on hyperpolarisation (termed ' $\text{I}_{\text{K}2}$ ' and originally thought to be the mechanism by which Purkinje fibres generated spontaneous depolarisation) [26, 27]. Hence, it acts to depolarise the AP as it reaches its most negative potentials. This begins a shallow upstroke of the AP during phase 4, bringing it into the range at which I_{CaT} is most active, -40 to -20 mV. I_{CaT} , also an inward current, acts to further depolarise the AP until the threshold for phase 0 (about -30 mV) is reached. Pacemaker myocytes have much lower expression of I_{Na} than those of the WM, and hence the phase 0 upstroke is significantly slower than in the WM.

The calcium clock refers to the effect that the Ca^{2+} released during the CICR cycle has on I_{NaCa} [21, 23]. The primary release of Ca^{2+} during the CICR cycle is due to the Ca^{2+} ions which enter the cell during an AP. However, the diastolic level of Ca^{2+} in the intracellular space is not zero and hence there will be some Ca^{2+} release during phase 4. This release of Ca^{2+} into the cytosol can activate I_{NaCa} , which removes Ca^{2+} from the cytosol and brings in 3 Na^+ ions for each Ca^{2+} ion. This therefore has a net flow of charge into the cell, and is therefore an inward current which can contribute to depolarisation of the potential. This may become particularly important if the affinity of the RyR to Ca^{2+} is increased and Ca^{2+} release is increased during diastole [21, 23].

Recent evidence suggests that both mechanisms play a role in pacemaking [28]. Certainly, inhibition of I_{f} significantly reduces heart rate and can even abolish pacing [22]. Modulation of the intracellular Ca^{2+} systems also affects heart rate [21, 23]. It is likely that the presence of I_{f} , I_{CaT} and the calcium clock is a protective mechanism, making the heart resilient to dysfunction of any of these aspects individually. A more detailed debate as to the primary pacemaking mechanisms of the heart can be found in Lakatta and DiFrancesco 2009 [29] (Fig. 2.8).

Fig. 2.8 Roles of the different pacemaking mechanisms. Schematic of a pacemaker action potential with the roles of the pacemaking currents labelled. The *arrows* indicate the phases in which each current primarily contributes to spontaneous depolarisation



2.3.6 Characterising Action Potentials

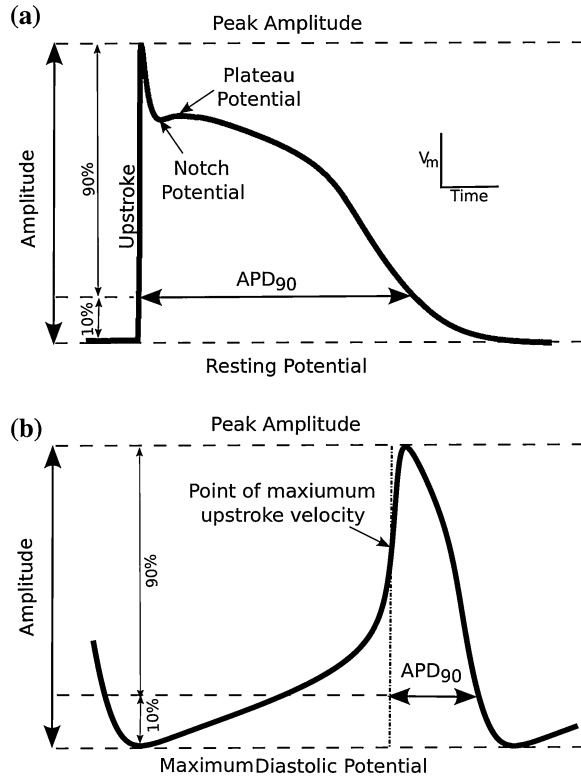
It is important to characterise APs in a consistent manner such that different APs can be analysed. This allows the APs from different regions, species or diseased states to be compared within a consistent framework. Figure 2.9a illustrates the properties of an excitable cell. The RP of an AP is related to the excitability of the myocyte and hence it is an important property to measure. The RP is the potential at which an excitable cell will remain if un-stimulated, and corresponds to the most negative potential. The upstroke is the first, fast depolarisation, corresponding to phase 0. It is common to measure the maximum upstroke velocity (MUV), which is the fastest rate of change of V_m during this phase. This is also related to excitability and has important implications on the conduction velocity of an AP in tissue. The peak amplitude is the most positive potential the AP reaches at the end of the upstroke. The amplitude of an AP is the difference between the peak amplitude and the RP. One of the most important concepts is the action potential duration (APD), which is a measure of the width (in time) of the AP. It is measured from the time of the upstroke until a specified percentage of total repolarisation. This specified percentage is subscripted to the APD. For example, the APD_{90} is the time between the upstroke and the time at which the AP first reaches below 90 % of the total amplitude. This example is highlighted in Fig. 2.9a. APD_{90} and APD_{95} are commonly used to assess the full width of the AP. APD_{30} and APD_{50} are also commonly used, often to assess the width of the plateau. It is, of course, possible to determine the APD at any percentage of repolarisation. Because the APD depends on the amplitude of the AP, the APD at a specific voltage is sometimes used. For example, the duration between the upstroke and when the AP reaches below -25 mV may be used. This is less common than the standard APDs, but can provide more information on aspects such as the prominence of the plateau when APs with different RPs or peak amplitudes (and hence amplitudes) are to be compared. In this thesis, such measurements will be denoted with the voltage as the subscript, for example, APD_{-25mV} .

Other properties commonly assessed are the notch potential and the plateau potential. These can provide more information on the shape of the AP itself. The notch potential is the most negative potential reached during phase 1 repolarisation and before phase 2. The plateau potential is the peak potential reached after the notch, during phase 2.

Characterising pacemaker cells has a couple of important distinctions. These are illustrated in Fig. 2.9b. First, there is no longer a stable RP. Instead, the maximum diastolic potential (MDP) is used, which refers to the most negative potential reached during a cycle. The amplitude is now the difference between the peak amplitude and the MDP. Also, the upstroke of the AP has a much shallower gradient. Hence, the APD is measured from the time at which the MUV occurs. This is also technically true of excitable cells, but due to the rate of change of V_m , this almost exactly corresponds to the line of the upstroke itself. It is also true that pacemaker cells do not have a notch or plateau potential.

Fig. 2.9 Characterising an AP. **a.** Characterising action potentials of the working myocardium.

b. Characterising pacemaker action potentials



2.3.7 Action Potential Propagation

The intercalated discs which connect adjacent myocytes contain gap junctional ion channels. These channels permit the transfer of ions between myocytes. Hence, when a myocyte is stimulated, ions in the intracellular space can flow into the adjacent myocyte. This can cause a depolarisation of the adjacent cell such that the threshold for the activation of I_{Na} is reached, and a full AP is initiated. It is this process which allows the AP to propagate through the CCS and the myocardium. The proteins responsible for gap junctions are known as connexins and denoted Cx. The major isoforms of connexins present in cardiac tissue are Cx40, Cx43 and Cx45. Cx43 is the most abundant and permits the fastest flow of ions between myocytes. Nodal tissue exhibits a lower expression of Cx43, which is partly responsible for the slower conduction within the SAN and AVN. However, the smaller myocyte size associated with nodal tissue also contributes to the slower conduction velocities.

Myocytes are arranged end to end longitudinally in fibres. Gap junctional channels are far more abundant in the connections between the ends of cells than the side. This means that excitation can travel much more quickly along a fibre

than perpendicular to it. The CCS contains a high degree of fibre organisation which contributes to the fast conduction velocities achieved within it. In general, the organisation of fibres in the atrial working myocardium (AWM) is far more disorganised than in the ventricles. It is thought that this contributes to the prominence of atrial arrhythmias.

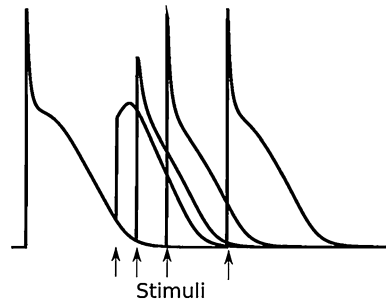
2.3.8 Action Potential Memory, Restitution and Re-entry

An important property of cardiac APs is related to memory. Memory refers to the effect that pacing rate and preceding APs has on the form of an initiated AP. During pacing at regular intervals, the size of the interval (or equivalently the rate of pacing) can affect properties such as the MUV, amplitude, plateau and APD. The time interval between successive stimuli is referred to as the basic cycle length (BCL). In simplified terms, shorter BCLs lead to a shorter APD and slower upstroke velocity. The relationship between BCL and APD is known as an APD restitution curve. The shape and gradient of the restitution curve can have important implications in arrhythmogenesis. At very high rates (those corresponding to or shorter than the APD_{90}) AP and Ca^{2+} transient alternans may be observed. This is when the APD_{90} or Ca^{2+} amplitude alternate between two (or more) different values, corresponding to a shorter and longer AP. The presence of alternans has large implications on arrhythmogenesis.

Applying a stimulus to tissue or individual myocytes at regular pacing intervals is known as an S1 protocol. An S1–S2 protocol refers to a case where a train of regular S1 stimuli are applied followed by a shortly coupled S2 stimulus. An S1–S2 protocol can highlight the memory properties of an AP: as the S2 coupling time shortens, the final AP produced demonstrates a reduced upstroke velocity, amplitude and APD. Below a threshold (usually within the APD_{90} at the S1 pacing rate), a full AP cannot be initiated. This is called the effective refractory period (ERP). An example of this is shown in Fig. 2.10. Here, 4 different cases of an S1–S2 protocol with different S2 timings are imposed on each other. The first AP is common to all four as they are paced at the same S1 rate. It can be clearly seen that as the S2 stimulus coupling time is reduced, the AP is markedly changed. This property is known as the refractoriness of an AP. Memory and refractoriness are related to both the inactivation gates of the ion channels (affecting whether a current can be re-activated) and the intracellular concentrations of the ions (the shorter the coupling, the less time is allowed for ion concentrations to be reset), as well as possible active K^+ currents if stimulated during the AP. Memory effects are one of the reasons it is important to measure APD.

One effect of refractoriness is to protect the heart against fast stimulation. If the heart were to be continuously stimulated at a high rate, the lack of time for relaxation would reduce the contractile ability of the myocyte and hence reduce cardiac output. Restitution means that fast stimuli may not be able to propagate through the tissue, and hence allows the heart relaxation time. Restitution also has

Fig. 2.10 Illustration of refractory properties of action potentials. Shown are traces corresponding to four S2 timings during an S1–S2 pacing protocol. The first AP is common to all four. *Arrows* indicate the time at which S2 stimuli are applied



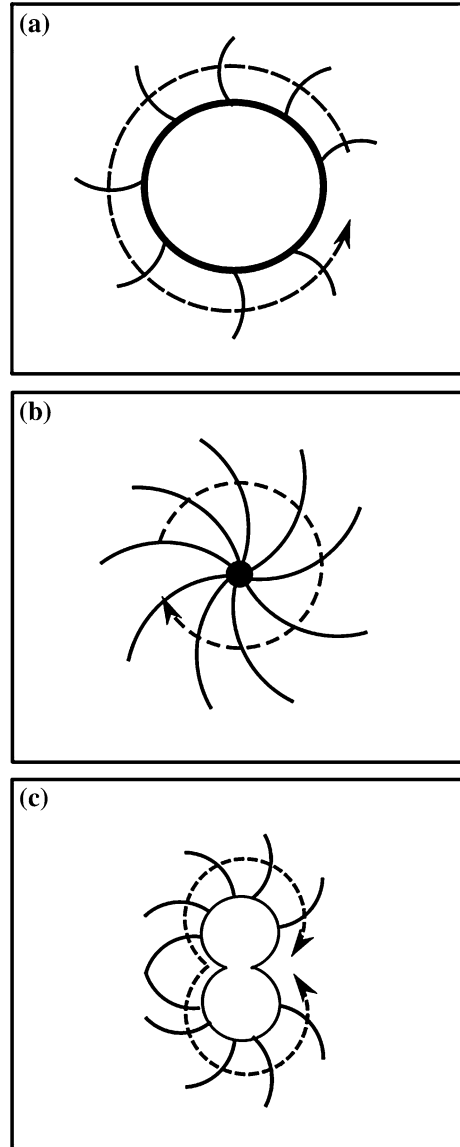
important implications on re-entry. Re-entry is the term given to a propagating wave which self sustains. This may occur in the form of spiral or scroll waves, or in leading circle re-entry (illustrated schematically in Fig. 2.11). Such propagation may provide high pacing rates and override the natural pacing from the SAN. Restitution is intimately linked to re-entry, in both anti-arrhythmic and pro-arrhythmic ways. It may help to terminate re-entry by the prevention of sustained propagation. However, restitution can also lead to uni-directional conduction block, in which propagation is blocked in one direction but not in the other. The presence of such conduction block provides functional barriers for wave propagation. This can lead to the breakup of a regular propagation wave and may lead to the initiation of re-entrant circuits.

The role of conduction block and the intimate relationship between ERP and re-entry can be illustrated by considering one of the mechanisms by which re-entry may be initiated. This is illustrated in Fig. 2.12. Consider the boundary between two regions of different ERPs. If an S1–S2 protocol is applied at the junction (indicated by the asterisk), and the S2 stimulus is timed such that it is between the ERPs of the two regions, then propagation may be blocked towards the region with the longer ERP (Fig. 2.12b). After some time, this region will have recovered, and the action potential will be permitted to propagate (Fig. 2.12c). The action potential will now propagate within this region towards the site of the initial stimulus. If sufficient time has passed such that the first region has recovered, the action potential will propagate back into the first region (Fig. 2.12d). Such a cycle may repeat indefinitely. In this example, it can be seen that the absolute ERP and the difference in ERP between the two regions defines whether a stable re-entrant circuit can be permitted.

2.4 Experimental Techniques

This section discusses a range of experimental techniques used to either characterise APs and currents or cardiac organ structures. The ElectroCardioGram (ECG), which is the most commonly used diagnosis tool, is discussed in Sect. 2.5.

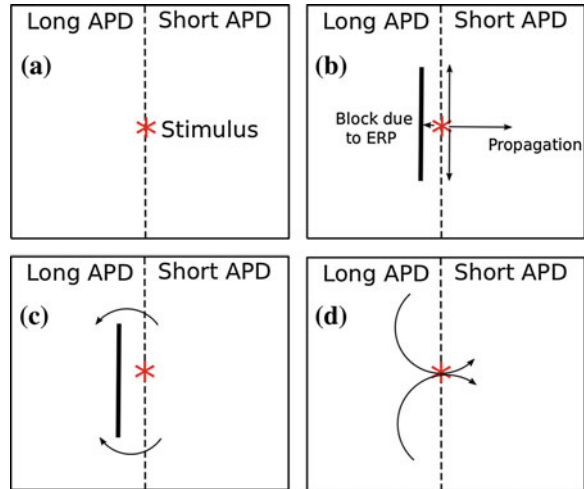
Fig. 2.11 Schematic of re-entry. Schematic example of three different types of re-entry. *Dotted arrows* indicate the direction of wavefront propagation. **a** Leading circle re-entry. Waves propagate in a circuit around a structural obstacle, such as the opening of a blood vessel into the heart. **b** Single spiral wave re-entry. Waves rotate around the spiral wave tip (*solid circle*). **c** Figure 2.8 re-entry. Two waves rotate in opposite directions, forming a figure-8



2.4.1 Voltage Clamp

Voltage clamping techniques (also referred to as patch clamps) provide a way to characterise the different ionic currents. This is achieved through measuring currents during a series of ‘step’ voltages. Electrodes are placed in the intracellular and extracellular spaces. These can provide a potential difference across the cell

Fig. 2.12 Illustration of a mechanism of re-entry. A schematic illustration of the link between ERP and re-entry. The *asterisk* indicates a stimulation site. The *dotted line* represents the boundary between two regions which exhibit a different APD and ERP, while the *solid line* indicates conduction block. *Arrows* indicate direction of wavefront propagation



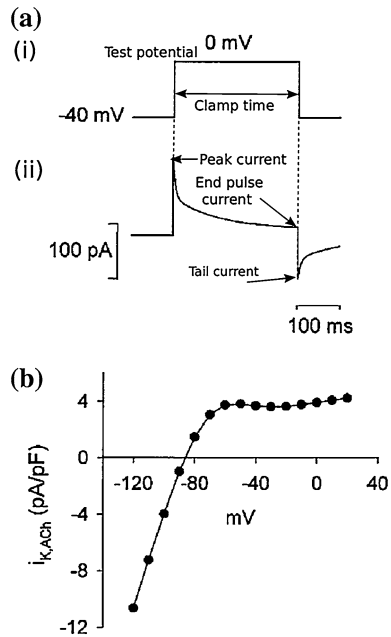
membrane and measure the resulting currents. In the simplest form, the membrane potential is first held at a holding voltage. It is then instantaneously stepped up to a ‘test potential’ for a certain amount of time, known as the ‘clamp time’. After this time, it is stepped back down to the holding potential (Fig. 2.13a-i). This is then repeated for different test potentials, usually in increments of 10 mV, somewhere in the range -140 to 60 mV. The exact range and clamp time is dependent on the current being measured. Either the peak current during the test potential, the current at the end of the test potential or the tail current (the current just after the voltage is stepped back to the holding potential) is returned (illustrated in Fig. 2.13a-ii). These data can be used to create a current–voltage (I–V) relationship: The current (whichever value is used) is plotted against the test potential (Fig. 2.13b). This provides an indication of the voltage ranges in which the current is most active. Please note, it does not directly imply the value of the current at various voltages during an AP, as most currents are time dependent.

2.4.2 Imaging Techniques

Imaging techniques can be used to extract and characterise complex anatomical and fibrous structure from segments of tissue or whole organs. These images can be used to create anatomically accurate geometrical structures which can be used in computer modelling or analysed to indicate structural diseases.

Magnetic Resonance Imaging (MRI) uses a process known as nuclear magnetic resonance to provide images of tissue or organs. A magnetic field is applied and measures of the changes to the spin of the hydrogen nuclei present in water can build up images of tissue structures. This then produces a series of coloured

Fig. 2.13 Voltage clamp example. **a** Example of a single voltage clamp step function (i) and the resulting current trace (ii). The different currents which may be returned are all labelled. **b** Example of an I–V relationship. The current (y-axis) is plotted against the test potential (x-axis). Adapted from [30]



voxels, where the colour (shades of grey) corresponds to the presence and thickness of tissue. Diffusion tensor MRI (DT-MRI) is a modification to MRI which uses magnetic gradients to extract fibre structure [31]. The gradients in the magnetic field cause water to flow. The speed and direction of this flow are measured for each voxel. As water is more likely to flow along a fibre than transverse to it, the information can be used to re-construct a full 3D map of the fibrous structure of the heart. DT-MRI is non-invasive and relatively quick compared to histology. It also has the advantage of leaving the tissue intact, and hence allowing it to be used for other purposes. It has been shown using histology that fibrous structure created using DT-MRI is valid [32, 33].

Computed tomography, also known as CT scan, uses a series of x-rays to build up an array of image slices. Like MRI, CT scans can also be used to create geometrical models of anatomy. Micro CT is a relatively new technique which has a higher resolution than CT scans. It can resolve to a small enough degree to pick up fibrous detail, to which an algorithm can be applied to create a model of fibre structure.

Optical mapping is a method which allows the activation sequence and APs to be measured in the intact heart or tissue. It relies on dyes whose colour is voltage dependent. By applying these dyes, the spread of electrical activity can be measured using optical cameras by monitoring the changes in the colour of the dyes [34–37]. The AP traces produced by this technique are not as detailed as those attained through the use of electrodes, but more detail is provided on the activation sequence than can be attained from electrode arrays.

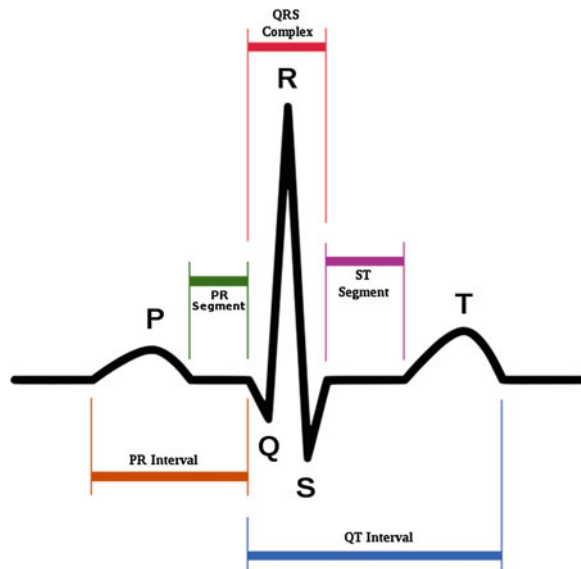
2.5 The ElectroCardioGram

The ECG is the most commonly used tool in the analysis and diagnosis of cardiac disorders. It is a relatively simple, non-invasive method that can provide detail on the electrical activity of the heart. It does so by measuring changes in the potential distribution on the surface of the body, which arise from the changes in electrical activity of the surface of the heart.

2.5.1 The ECG Waveform

A typical ECG is made up of various different waves, corresponding to the depolarisation and repolarisation of the atria and ventricles. A labelled schematic of an ECG is shown in Fig. 2.14. The P-wave is the first deviation observed in an ECG and corresponds to the depolarisation of the atria. This is followed by the T_p wave (not labelled), which corresponds to the repolarisation of the atria. The T_p wave is inverted compared to the P-wave, and is usually not observed in clinical ECGs. This is because it is often obscured by the QRS complex. The QRS complex represents the depolarisation of the ventricles. Because the ventricles have a much larger mass than the atria, the QRS complex is usually an order of magnitude larger than the P-wave. Finally is the T wave, which is due to repolarisation of the ventricles. Due to ventricular APD heterogeneity, it is usually in the same orientation as the QRS complex.

Fig. 2.14 Schematic of an ECG. A schematic example of a typical ECG waveform. The different waves and intervals are labelled. Adapted from [38]



2.5.2 Analysing ECGs

There are various properties of the ECG which can be analysed to indicate either healthy or diseased states in the heart. Below are described just a few of these properties.

I. *PR interval*

The PR interval is the time between the start of the P-wave and the first deflection of the QRS complex. It represents the time taken for excitation to conduct from the SAN and through the AVN to the ventricles. Whereas the width of the P-wave can indicate atrial conduction, the PR interval is an indication of AV-nodal function. A prolonged PR interval combined with a normal P-wave duration can suggest AV-nodal block. Normal PR intervals are between 120 and 200 ms [39, 40].

II. *PR ratio*

The PR ratio refers to the number of QRS complexes associated with each P-wave. In the healthy heart, this ratio is 1:1, because each activation of the atria leads to an activation of the ventricles. However, AV-node block can result in ratios larger than this, in which each activation of the atria does not lead to an activation of the ventricles. During periods of fast pacing atrial pacing, for example, the longer APDs in the AVN will prevent propagation of atrial activation into the ventricles, and ratios of 2:1 or greater may be observed.

III. *RR interval*

The RR interval is the time between successive R waves. It is therefore a direct measure of the heart rate. In the healthy heart, this will also be equivalent to the PP interval.

IV. *Polarity of T wave*

Unlike the T_p -wave, which is inverted in relation to the P-wave, the ventricular T-wave may be in the same orientation as the QRS complex. Repolarisation heterogeneities within the ventricular wall and along the extent of the ventricles result in repolarisation patterns propagating in the opposite direction to depolarisation patterns in human [41]. An inversion of the T-wave may suggest the presence of abnormal heterogeneity.

V. *Saw tooth waves*

‘Saw tooth’ ECGs are observed during times of rapid pacing. This may occur during a tachycardia or fibrillation state. If it is regular, this suggests tachycardia, which may be the result of a regular but fast spinning rotor wave. During fibrillation, highly chaotic saw tooth waves are observed [43].

2.5.3 The 12-Lead ECG

The standard 12-lead ECG uses 9 electrodes (Fig. 2.15), which combine to form 12 leads (Eqs. 2.2–2.13). Electrodes measure a potential, and the leads measure a potential difference, derived from the differences between electrodes. The first three electrodes correspond to the ‘Einthoven Triangle’. The electrodes are placed at the corners of a triangle in which the heart sits—one on the left arm (L or LA), one on the right arm (R or RA) and one on the left leg (F or LL) (Fig. 2.15a). The leads are measured along the sides of this triangle, corresponding to the differences between the electrodes. These are the three limb leads, leads I–III (Eqs. 2.2–2.4). From these electrodes is also derived the Wilson’s Central Terminal (WCT) [44]. This is an average of the potentials at each of these electrodes, and is used in the derivation of many of the other leads (Eq. 2.14). The next 6 electrodes are placed over the chest in the vicinity of the heart, as in Fig. 2.15b, and are denoted as electrodes V_{1-6} . The leads derived from these electrodes are known as the precordial leads. They are constructed using the electrode as the positive and the WCT as the negative (Eqs. 2.5–2.10). For the remainder of this thesis, V_{1-6} refers to the leads, rather than the electrodes, unless explicitly stated. The final three leads are known as the augmented limb leads. These were originally constructed in a similar manner to the precordial leads, with the electrode of interest as the positive and the WCT as the negative. However, it was found that removing the contribution of the lead of interest from the WCT helped to amplify the wave [45]. Hence, the lead definitions are as follows:

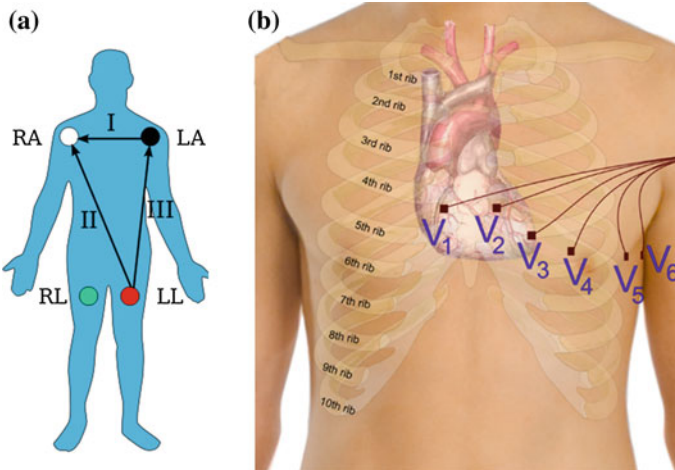


Fig. 2.15 Electrode placement in the 12 lead ECG. **a** Placement of the limb electrodes on the body. RL corresponds to the ground electrode, and does not contribute to any of the leads. Leads I–III are indicated by the arrows. **b** Placement of the precordial electrodes on the chest. Adapted from [42]

$$I = \phi_{LA} - \phi_{RA} \quad (2.2)$$

$$II = \phi_{LL} - \phi_{RA} \quad (2.3)$$

$$III = \phi_{LL} - \phi_{LA} \quad (2.4)$$

$$V_1 = \phi_{V1} - WCT \quad (2.5)$$

$$V_2 = \phi_{V2} - WCT \quad (2.6)$$

$$V_3 = \phi_{V3} - WCT \quad (2.7)$$

$$V_4 = \phi_{V4} - WCT \quad (2.8)$$

$$V_5 = \phi_{V5} - WCT \quad (2.9)$$

$$V_6 = \phi_{V6} - WCT \quad (2.10)$$

$$aVR = \phi_{RA} - \frac{\phi_{LA} + \phi_{LL}}{2} \quad (2.11)$$

$$aVL = \phi_{LA} - \frac{\phi_{RA} + \phi_{LL}}{2} \quad (2.12)$$

$$aVF = \phi_{LL} - \frac{\phi_{LA} + \phi_{RA}}{2} \quad (2.13)$$

where

$$WCT = \frac{\phi_{LA} + \phi_{RA} + \phi_{LL}}{3} \quad (2.14)$$

And ϕ_x is the potential recorded at electrode x.

2.6 Autonomic Regulation of the Heart

The activity of the heart can be regulated through the nervous system by the release of hormones which interact with the electrophysiology of the myocytes [46–50]. The hormones in the body can have many different effects in different regions. In the heart, the most relevant to this thesis are those released by the sympathetic and parasympathetic regulatory systems. Sympathetic regulation refers to the release of isoprenaline (ISO), a structural isomer of adrenaline. It acts to increase the spontaneous pacing rate of the pacemaker regions and is responsible for the increased heart rate during the ‘fight or flight’ response. It also affects the morphology of the APs in the working myocardium. ISO affects many of the ion channels and SR processes in the myocyte. It has been suggested to have

proarrhythmic properties. A detailed description of the electrophysiological affects of ISO is discussed in [Sect. 5.1.2](#).

The parasympathetic regulatory system involves the release of acetylcholine, ACh, which has the opposite effect on the pacemaker potentials as ISO; that is, it reduces the pacing rate [30]. It also shortens the APs by the activation of the acetylcholine activated potassium channel, $I_{K_{ACh}}$. The roles that ISO and ACh may play in the healthy and diseased heart is investigated in this thesis, in [Chaps. 5](#) and [7](#).

2.7 Cardiac Arrhythmias and Diseases

Arrhythmia literally means ‘without rhythm’. In the context of the heart, it refers to any period in which there is either no rhythm or an irregular rhythm. Arrhythmias mean irregular contraction, which leads to reduced cardiac output and can in some cases lead to death. Many cardiac diseases are a result of or lead to arrhythmias in some way. The range of cardiac diseases is extensive, described below are just a few of the main and most common ones. It is worth noting that many of the cases described below are often not distinct from each other.

2.7.1 Bradycardia

Bradycardias refer to slow heart rates. They can arise due to the effect of the parasympathetic regulatory system, or be indicative of an underlying problem. Trained athletes often exhibit bradycardias, sometimes to severe proportions. Severe bradycardias can lead to a reduction in the amount of nutrients and oxygen delivered around the body, which may have dangerous implications and can put strain on the organs. They are also associated with sinus exit and AV-nodal block.

2.7.2 Tachycardia

Tachycardias refer to fast activation of the heart. They can be a result of the presence of a fast pacing ectopic focus or the presence of re-entrant spiral waves. High rates of pacing are associated with reduced cardiac output, which can predispose to heart attack. Persistent tachycardias are associated with electrical and structural remodelling of the heart, and can lead to fibrillation.

2.7.3 Fibrillation

Fibrillation refers to fast and irregular activation of the heart. As with tachycardias, fibrillation is associated with the presence of re-entrant spiral waves. It characterised by the presence of multiple re-entrant spiral waves, which lead to a serious reduction in the coordinated contraction of the heart and hence cardiac output. Fibrillation can be distinguished from tachycardia due to its more irregular conduction patterns and ECG waveforms. Atrial fibrillation is the most common sustained cardiac arrhythmia [51], and may persist for long periods of time. Ventricular fibrillation almost immediately leads to a heart attack and can result in death. Atrial fibrillation can predispose to ventricular fibrillation, heart attack, stroke and even sudden death [52, 53].

2.7.4 Ischemia

Ischemia refers to regions of the heart in which cell death has occurred, usually due to a lack of blood flow to the region. The presence of such regions can lead to reduced cardiac output, as these regions no longer contract. They can also provide structural obstacles which can contribute to the break-up of regular propagation waves and lead to re-entry. Hence, ischemia can predispose to tachycardia and fibrillation.

2.7.5 Genetic Mutation Induced Cardiac Arrhythmias

Most gene mutations which occur have no significant effect on impairing cardiac functions. However, some gene mutations can result in dysfunction of different properties of the heart. For example, mutations in the HCN isoforms which code for I_f can lead to severe bradycardias and AV-node block [54]. Similarly, mutations in SCN5A, which codes for I_{Na} , can lead to reduced excitability of the heart and may lead to sinus node exit block [55].

2.8 Mathematical Electrophysiology

In order to develop computational models of cardiac cells and organs, the processes already described must be formalised mathematically. In 1952 Hodgkin and Huxley published the first mathematical model of an AP in the squid giant axon [56]. Their approach to the formulations of the ionic currents due to passive ion channels is one of the methods still used today and is described below in

Sect. 2.8.3. However, one aspect of their model has wider applications and is used as the base concept for all mathematical models of APs. This was the idea that the cell membrane and ionic currents can be represented by different electrical components making up a simple electric circuit (Sect. 2.8.1). Denis Noble first used Hodgkin-Huxley style equations to describe cardiac action potentials in 1962 for the canine Purkinje fibre [57].

2.8.1 Electric Circuit Model

The membrane itself separates charges and hence can be represented as a capacitor. The ion channels, pumps and exchangers allow current to flow through them, driven by a voltage dependent on the membrane potential and have an associated resistance (or conductance) which can vary with time and voltage. Hence, they can be represented as variable resistors. Each channel, pump or exchanger is independent of the others and hence they can be aligned in parallel (Fig. 2.16). From this concept, it only requires the application of Ohm's law and Kirchoff's laws to arrive at important equations which can relate the ionic currents to the changes in transmembrane potential.

Kichoff's first law states that the total ionic current (the sum of all of the ionic currents, I_{ion}) and the capacitive current (I_{cap}) must sum together to equal zero:

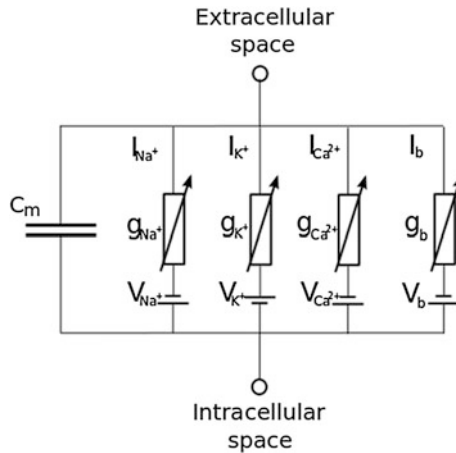


Fig. 2.16 Electric circuit model of the cell membrane. Schematic diagram of the structure of the electric circuit model of the membrane. This particular example has a Sodium, Potassium Calcium and background current, aligned in parallel. The membrane is represented by a capacitor, and the membrane capacitance denoted C_m . The conductance of each channel is labelled as g_x . The V_x term in each channel is the electromotive force driving the current flow across the channel

$$I_{cap} + I_{ion} = 0 \quad (2.15)$$

And therefore that

$$I_{ion} = -I_{cap} \quad (2.16)$$

The capacitor relation (Eq. 2.17) can then be used to relate the ionic currents to the changes in transmembrane potential (the AP) by differentiating it with respect to time:

$$Q = C_m V_m \quad (2.17)$$

$$\frac{dQ}{dt} = \frac{d}{dt}[C_m V_m] \quad (2.18)$$

Assuming that the membrane capacitance is not a function of time, this leads to:

$$I_{cap} = C_m \frac{dV_m}{dt} \quad (2.19)$$

Equating Eq. (2.16) with Eq. (2.19) and rearranging relates the change in transmembrane potential to the total ionic current as such:

$$\frac{dV_m}{dt} = \frac{-I_{ion}}{C_m} \quad (2.20)$$

This equation can then be integrated to determine the AP. It is now necessary to derive a form for the ionic currents. Ion channels are the simplest form as they are dependent on passive processes. It is their formulation which is described here. This can be done using Ohm's law (Eq. 2.21). It is conventional to use the conductance, g , rather than the resistance, related by Eq. (2.22).

$$V = IR \quad (2.21)$$

$$g = 1/R \quad (2.22)$$

$$I = gV \quad (2.23)$$

It is important to note that V here is not the transmembrane potential, but a driving force to the ionic currents. Each of the individual ionic currents can be formulated in this general way, and then summed to give the total ionic current. The form of g and V must now be discussed. The driving force, V , is formulated in a common way in mathematical models and is related to the Nernst equilibrium potential, discussed below. It is in the formulation of g , the conductance of the channel, that different approaches can be taken. The most common are the Hodgkin Huxley approach (Sect. 2.8.3) and Markov chain models (2.8.4).

2.8.2 Nernst Equilibrium Potential

The Nernst equilibrium potential, also known as the reversal potential, and denoted E_r , is the potential at which the electric force, due to the charge gradient, and the chemical force, due to the concentration gradient, across the cell membrane are of equal magnitude and in opposite directions [58]. Hence, at this potential the electrochemical force on an ion is zero. This means that there is no net flow of charge through a passive ion channel, and hence the current is also zero. It is given by:

$$E_{ion} = \frac{RT}{zF} \ln \left(\frac{[ion]_e}{[ion]_i} \right) \quad (2.24)$$

where E_{ion} is the Nernst equilibrium potential, R is the universal gas constant, T is the absolute temperature (in Kelvin), F is Faraday's constant, Z is the valence number (corresponding to the charge on the ion) and $[ion]$ refers to the concentration of the ion in the extracellular (e) and intracellular (i) spaces.

This is particularly useful as it allows the driving force behind such passive processes to be formulated purely electrically: the difference between the transmembrane potential and the reversal potential will act as an electromotive force on the ion. This provides a form for the V term in Eq. (2.23), and hence the ionic current is given by:

$$I_{ion} = g(V_m - E_{ion}) \quad (2.25)$$

2.8.3 Hodgkin Huxley Type Formulations

Hodgkin and Huxley formulated two time and voltage dependent currents (a Na^+ and a K^+ current) and one time independent leak current [56]. The mathematical approach and assumptions used are still used today. The gross kinetics of an ion channel are modelled through the use of activation and inactivation variables, corresponding to the activation and inactivation gates. It is assumed that the activation and inactivation gates are independent of each other. The activation variable corresponds to the fraction of channels that are in the activated state. Hence, a value of 0 represents none of the channels being activated, and a value of 1 represents all of them being activated. The inactivation variable corresponds to the fraction of channels that are not in the inactivated state. Hence, a value of 0 represents all of the channels being in the inactivated state and a value of 1 means none of them are. Therefore, multiplying these two variables together describes the fraction of channels that are in the open state (activated and not inactivated) and hence the proportion of the maximum current that flows. Hence, the general form for an ionic current is given by:

$$I_{ion} = m^a h^b g_{max} (V_m - E_{r_{ion}}) \quad (2.26)$$

where m and h are gating variables and g_{max} is the maximum conductance of the channel. Here, the powers of the gating variables, a and b , are present to empirically fit the form of the gates observed experimentally. Hodgkin and Huxley drew an analogy to the power representing the number of particles that must be in a certain position for activation or inactivation to occur. If activation requires 3 separate particles to be in position, then the probability of the channel being in the activation state is the cube of the probability of each particle being in that state. It is worth noting that there is no reason why just two types of gate must be present: some potassium channels do not feature inactivation and hence have just an activation variable. Similarly, some channels exhibit two distinct time courses of inactivation or activation, and this can be modelled using two separate inactivation/activation gates which have different properties.

This approach allows both voltage and time dependence to be incorporated. Consider an activation gating variable, y . The value of y represents the proportion of channels in the activated state (or equivalently, the proportion of activation gates that are open). Hence, the proportion of channels not in the activated state (or the proportion of activation gates which are closed) must be $(1 - y)$. Rate coefficients, α_y and β_y are related to the transitions between these two states. If α_y is related to the opening of the gate, then the rate of change of opening will be given by $\alpha_y(1 - y)$. Similarly, the rate of change of closing will be described by $\beta_y y$. This corresponds to a transition equation of the form:

$$(1 - y) \xrightleftharpoons[\beta_y]{\alpha_y} y \quad (2.27)$$

And hence the rate of change of y is described by the following differential equation:

$$\frac{dy}{dt} = \alpha_y(1 - y) - \beta_y y \quad (2.28)$$

If the values of either α_y or β_y depend on V_m , then the state of the gate will be voltage dependent as well as time dependent. It is sometimes more useful to change the form of this equation (Eq. 2.29). This is known as the steady state of the gate, and represents the value to which the gating variable will tend at a certain voltage. If the voltage is instantaneously changed, the rate at which the gate will approach its steady state value for the new voltage is described by the time constant, given by Eq. (2.30).

$$y_{\infty} = \frac{\alpha_y}{\alpha_y + \beta_y} \quad (2.29)$$

And

$$\tau_y = \frac{1}{\alpha_y + \beta_y} \quad (2.30)$$

where y_∞ is the steady state value of the gate y and τ_∞ is the time constant.

These can be useful as they can give a better indication of the activity of a channel at a certain voltage, and a measure of its ability to respond to changes in potential. For this reason, they are easier to interpret. The differential equation describing the gating kinetics is now:

$$\frac{dy}{dt} = \frac{y_\infty - y}{\tau_y} \quad (2.31)$$

It is common experimentally and in modelling studies to measure and fit the steady state values and time constants directly. The steady state values often take the general form of a simple sigmoidal function, such as:

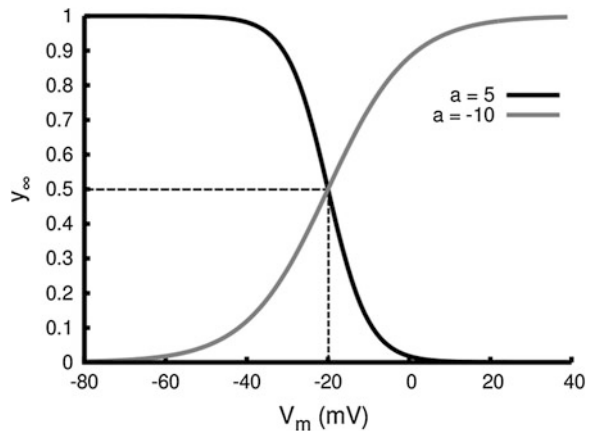
$$y_\infty = \frac{1}{1 + \exp(V_m - V_{1/2}/a)} \quad (2.32)$$

where $V_{1/2}$ is the voltage of half activation, a is the gradient of activation and all other parameters retain their previous meaning. Both $V_{1/2}$ and a are determined empirically, and a may be negative or positive.

Figure 2.17 shows two examples of functions of this type. Both have a $V_{1/2}$ of -20 mV, and it can be seen that at this voltage the steady state value of the gate is 0.5 (dotted line). The effect of the sign and magnitude of the gradient, a , can also be clearly seen. From the steady state value (y_∞) and τ_y , α_y and β_y can be extracted using the following equations:

$$\alpha_y = \frac{y_\infty}{\tau_y} \quad (2.33)$$

Fig. 2.17 Steady state gating variable example. Example of the relationship between the steady state value of a gating variable and membrane potential. Shown are two examples, both of which have a $V_{1/2}$ of -20 mV, indicated by the dotted line. The sign of the gradient (a) determines the direction of the variable



$$\beta_y = \frac{(1 - y_\infty)}{\tau_y} \quad (2.34)$$

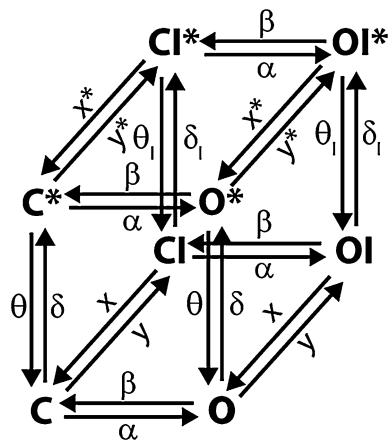
Using this formalism, the time course of the gating variable is defined by:

$$y = y_\infty - (y_\infty - y_0) \exp\left(\frac{-t}{\tau_y}\right) \quad (2.35)$$

2.8.4 Markov Chain Models

Markov chain models are an alternative method of expressing the conductance, g , in Eq. (2.25). Similar to Hodgkin-Huxley type formulations, the maximum conductance is multiplied by a number between 0 and 1 to describe the proportion of the maximum current which flows. However, instead of expressing a channel in terms of different gates, which are either open or closed, the state of the channel is expressed in terms of a chemical transition formulation. This describes the different conformational states of the channel. An example of such a structure is shown in Fig. 2.18. With this type of model, the gating parameters in Eq. (2.26) are replaced by the sum of the open states (states O and O* in the figure). It is assumed in Hodgkin-Huxley formulations that the activation and inactivation states are independent of each other. However, this is not the case, and Markov models contain this interdependence. A disadvantage of Markov chain models is that they contain a larger set of equations and are hence more computationally intensive to solve. For this reason, it is common practice to only use Markov chain models when Hodgkin-Huxley formulations do not fit the data. This may be the case when modelling a mutation (such as in the Adeniran et al. 2011 model of short QT syndrome [60]) or the action of a regulatory pathway (such as in the

Fig. 2.18 Example of a Markov chain model. An example of a Markov chain model, in this case for I_{CaL} . The channel is open when in state O or O*. The symbols by the arrows are the transition rate constants describing the transition from one state to another, similar to α and β in the Hodgkin-Huxley type equations. Adapted from [59]



Heijman et al. 2011 model of the effect of isoprenaline in the canine ventricular myocyte [61]).

2.8.5 AP Propagation

It is impractical to model the gap junctions explicitly. Instead, a continuum approach is used. If it is assumed that the intracellular and extracellular conductivities are the same, the propagation of the AP can be described using the monodomain equation [62–64]:

$$\frac{\partial V}{\partial t} = \nabla \cdot \mathbf{D}(\nabla V) - \frac{I_{ion}}{C_m} \quad (2.36)$$

where \mathbf{D} is the tensor of diffusion coefficients, which characterises the rate of spread of the electrical activity, ∇ is the 3D spatial laplacian defined within the tissue, V is the membrane potential, I_{ion} is the total ionic current and C_m is the membrane capacitance. As cardiac tissue is fibrous in structure, and propagation is faster along the fibre than transverse to it, the components of \mathbf{D} in a local coordinate system (aligned along the fibre direction, denoted $\tilde{\mathbf{D}}$) will be heterogeneous, and represented by the diagonal matrix:

$$\tilde{\mathbf{D}} = \begin{pmatrix} D_{\parallel} & 0 & 0 \\ 0 & D_{\perp 1} & 0 \\ 0 & 0 & D_{\perp 2} \end{pmatrix} \quad (2.37)$$

where D_{\parallel} , $D_{\perp 1}$ and $D_{\perp 2}$ are the diffusion coefficients along the fibre axis, transverse to it and across the sheet. In the atria, where there is no conclusive evidence of the sheet structure found in the ventricles, $D_{\perp 1}$ and $D_{\perp 2}$ are equal to each other, and are usually 5–20 times [64, 65] smaller than D_{\parallel} . It is necessary to transform $\tilde{\mathbf{D}}$ such that it applies not in a local coordinate system orthogonal to the fibre direction, but instead in a global coordinate system, consistent across the whole tissue. This is achieved with a standard transformation, as such:

$$\mathbf{D} = \mathbf{A}\tilde{\mathbf{D}}\mathbf{A}^T \quad (2.38)$$

where \mathbf{A} is a matrix derived empirically from the fibre direction eigenvectors as such:

$$\mathbf{A} = \begin{pmatrix} \mathbf{f} & 0 & 0 \\ 0 & \mathbf{s} & 0 \\ 0 & 0 & \mathbf{n} \end{pmatrix} \quad (2.39)$$

where \mathbf{f} , \mathbf{s} and \mathbf{n} are an orthogonal set of vectors in which \mathbf{f} points along the fibre direction, \mathbf{s} points transverse to the fibre in the sheet direction and \mathbf{n} is normal to the sheet direction.

The monodomain equation reduces in 1D to the cable equation:

$$\frac{\partial V}{\partial t} = D \left(\frac{d^2 V}{dx^2} \right) - \frac{I_{ion}}{C_m} \quad (2.40)$$

where here D is a scalar value characterising the speed of propagation along the 1D strand.

2.9 Numerical Methods

Numerical methods describe ways in which continuous equations may be discretised such that they can be solved in an iterative manner on a computer. There are many numerical methods available, suitable for a whole range of different problems. In this section are only described those which are used in the models developed in this thesis.

2.9.1 Explicit Euler Method

The explicit Euler method, or forward Euler (FE) method, is the simplest numerical algorithm for the integration of differential equations. Consider a differential equation of the form:

$$\frac{dy}{dt} = f(y, t) \quad (2.41)$$

Such as is found in the gating variables for the current formulations and the membrane potential itself. It is assumed that over a small enough time interval, Δt , the rate of change of the variable, y , is constant. The change in the value of the variable over this time interval will therefore be:

$$\Delta y = \Delta t \times f(y, t) \quad (2.42)$$

The value of the variable at a time $t + \Delta t$ is given by:

$$y_{t+\Delta t} = y_t + \Delta y \quad (2.43)$$

And therefore:

$$y_{t+\Delta t} = y_t + \Delta t \times f(y, t) \quad (2.44)$$

If the initial values, (y_0, t_0) , are known then the value at the first time step, after one interval Δt , is given by:

$$y_1 = y_0 + \Delta t \times f(y_0, t_0) \quad (2.45)$$

And therefore more generally:

$$y_{n+1} = y_n + \Delta t \times f(y_n, t_n) \quad (2.46)$$

Hence, the succession of values $y_0, y_1 \dots y_n$ provides an approximation to the function over the time interval $\Delta t \times n$, providing Δt is sufficiently small.

The FE method is simple and hence computationally efficient. It is however limited by a very small time step due to the ‘crudeness’ of its integration method. More complex integration methods may be used, such as the 4th order Runge–Kutta method, which takes four estimations between times steps and averages them. These methods are better suited to highly stiff equations and allow larger time steps to be used without loss of accuracy. This can mean they can be computationally less intensive: they require more calculations per time step, but the larger time step may mean that fewer calculations need to be performed overall. However, the very fast action of the fast activation gate for the sodium channel provides a constraint on the size of the time step independent of the method used. This constrains the time step to within the bounds for which FE is appropriate. For this reason, the FE is the most commonly used method in cardiac modelling, and it has been previously shown that the errors induced through the use of the FE method in the context of the cardiac AP are minimal [66].

2.9.2 Finite Difference Method

The finite different method (FDM) is a relatively simple and commonly used method of discretising the monodomain equation to update the voltage of a myocyte within a geometry. It is simplest to explain in 1D. If it is assumed that the nodes (or myocytes) are aligned in a 1D strand with equal spacing Δx , then an approximation to the spatial term of the cable equation (Eq. 2.40) is:

$$D \frac{d^2 V}{dx^2} \approx \frac{D}{\Delta x^2} (V_{x+\Delta x, t} + V_{x-\Delta x, t} - 2V_{x, t}) \quad (2.47)$$

where D is the same as in Eq. (2.40), $V_{x, t}$ is the voltage of the node for which the voltage is being calculated at time t and $V_{(x \pm \Delta x, t)}$ is the voltage at the nodes at a distance Δx on either side at time t . Hence the change of membrane potential with time is given by:

$$\frac{dV}{dt} \approx \frac{D}{\Delta x^2} (V_{x+\Delta x, t} + V_{x-\Delta x, t} - 2V_{x, t}) - \frac{I_{ion}}{C_m} \quad (2.48)$$

Applying the FE method gives the value of V at a time $t + \Delta t$ as:

$$V_{t+\Delta t} = V_t + \frac{D\Delta t}{\Delta x^2} (V_{x+\Delta x, t} + V_{x-\Delta x, t} - 2V_{x, t}) - \frac{\Delta t I_{ion}}{C_m} \quad (2.49)$$

It is common when using the FDM in cardiac tissue for the space step to be equal in all three dimensions.

The term $D\Delta t/(\Delta x)^2$ is related to stability, and must remain <0.5 for convergence to occur [67]. It is worth noting that this also places a constraint on the time step used for the integration, providing further justification for using FE over more complex numerical techniques. It also constrains the size of spatial step, Δx . It is always good practice when solving such problems to test the convergence of the solution at the temporal and spatial steps used.

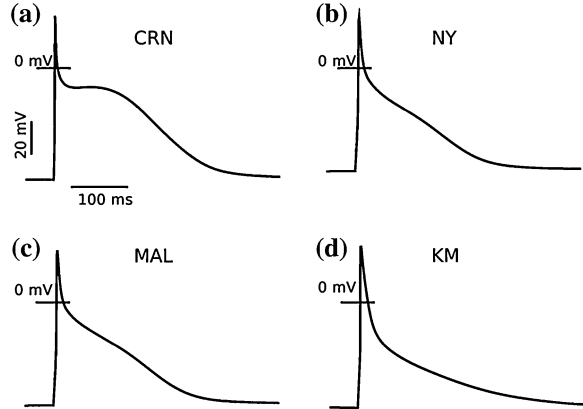
There are other methods available to solve the spatial diffusion of the AP. The most commonly used in cardiac simulations is the finite element method, FEM. This method may be more robust but can be more difficult to interpret, which can be important for debugging and for code intended to be used by others. Evidence has shown that both the FDM and FEM are appropriate for use for cardiac modelling. The FEM becomes necessary if the mechanical contraction is modelled, as the geometry needs to distort. Other alternatives include the boundary element method, the discrete element method and the finite volume method.

2.10 Human Atrial Myocyte Models

There are currently several models available describing the AP of human atrial myocytes. Only four of these models are discussed in detail in this section. The Courtemanche-Ramirez-Nattel (CRN) 1998 model [19] and the Nygren et al. (NY) 1998 model [68] were the first to be published. Both modelled the same ion currents and included intracellular handling systems. However, the data on which they were based was different and they exhibited distinct AP morphologies: The CRN model demonstrated a spike and dome morphology whereas the NY was significantly more triangular in shape. Recently, two updates to the NY model have been published. First, the Maleckar et al. (MAL) 2009 model [69] introduced new formulations for the K^+ currents I_{to} and I_{Kur} based on recent human data [70, 71]. Second, the Koivumäki et al. (KM) 2011 model introduced a new Ca^{2+} handling system [72]. There has also been an independent model developed in Grandi et al. 2011 [73]. In this section, a brief discussion comparing the CRN, NY, MAL and KM models in terms of their morphology, restitution, Ca^{2+} transients, comparison to experimental data and behaviour during remodelling is performed. The Grandi model is not considered here because it is based on a set of equations with high stiffness. For this reason, it relies on complex solvers and is very slow compared to the other models. Hence, it is not suitable for large scale simulations or 3D models designed to be easily portable. This is not a comment on the quality of the model itself, and is only a consideration based on the requirements of this thesis. A more detailed comparison of the CRN and NY models in single cell and tissue can be found in two papers published by Cherry et al. in 2008 [74, 75].

Fig. 2.19 AP morphology of human atrial myocyte models. Action potential traces produced by each of the four human atrial AP models, taken at a cycle length of 700 ms.

a Courtemanche-Ramirez Nattel model, **b** Nygren model, **c** Maleckar model, **d** Koivumaki model. The scale bars in **a** apply to all four panels



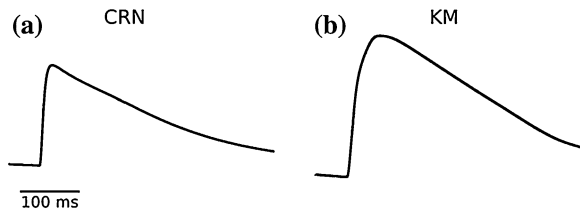
2.10.1 AP Morphology

The morphology of the four different AP models is shown in Fig. 2.19. The CRN model is the only one which exhibits a ‘spike and dome’ morphology. The NY and MAL models have very similar triangular morphologies. A small hump is observed, distinguishing phases 2 and 3. The KM model has a significantly lower notch potential than the other models, and also contains a wider phase 1. The resting potential (RP) of the CRN model is -80 mV, compared to -72 mV of the NY and MAL models, and -75 mV of the KM model. The CRN model has the longest APD_{50} (133 ms compared to 52, 42 and 27 ms of the MAL, NY and KM models respectively, at a BCL of 700 ms) due to its much more present dome, and also has the longest APD_{90} (263 ms compared to 220, 210 and 233 ms of the MAL, NY and KM models, respectively).

2.10.2 Calcium Transients

The shape of the Ca^{2+} transient in the CRN and KM models is shown in Fig. 2.20. The KM model is an improvement to the NY model and hence the NY and MAL model Ca^{2+} transients have been omitted from this figure. The Ca^{2+} transient in the CRN model exhibits a fast, single phase upstroke and a sharp point (Fig. 2.20a). The KM model exhibits a slower, two phase upstroke and a more rounded tip (Fig. 2.20b). This more closely replicates those observed experimentally [73, 76, 77]. The KM model also has a greater dependence on the sarcoplasmic reticulum Ca^{2+} release than does the CRN model.

Fig. 2.20 Ca^{2+} transients from the human AP models. Ca^{2+} transient during an AP from the CRN model (a) and the KM model (b). The scale bars in a apply to both panels



2.10.3 APD Restitution

APD restitution curves for the APD_{90} of the four models are shown in Fig. 2.21. It is worth noting that below a BCL of 350 ms, the KM model exhibits AP and Ca^{2+} alternans, which appear in the other models at lower BCLs. The APD restitution curve for the NY based models (NY, MAL and KM) don't demonstrate the rate dependency of the gradient of the curve as does the CRN model. At BCLs below 500 ms, the CRN model demonstrates the greatest rate dependency, as is observed experimentally [78, 79].

2.10.4 Stability

All of the models exhibit concentration and APD drift over long periods of time. However, the NY and MAL models are the most prone to stability issues: The RP, action potential amplitude, Ca^{2+} transient and APD_{90} all drift significantly over reasonably short simulation times. The CRN model is much more stable and only exhibits significant drift over very long simulation times.

The new Ca^{2+} handling system introduced in the KM successfully solves the stability issues present in the NY and MAL models.

Fig. 2.21 APD restitution of the four models. Cycle length dependency of the APD_{90} demonstrated for all four models: CRN (solid black line), NY (dotted black line), MAL (solid grey line) and KM (dotted grey line)

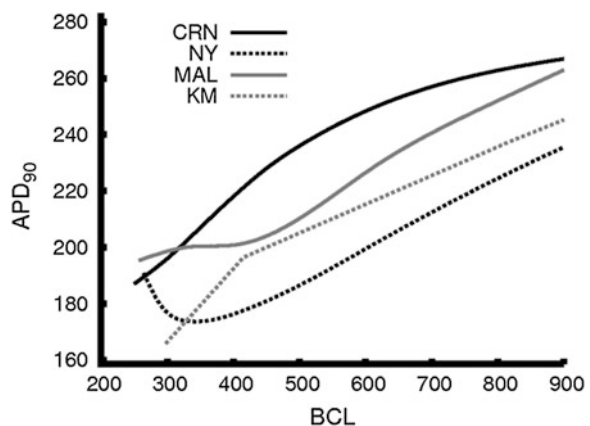
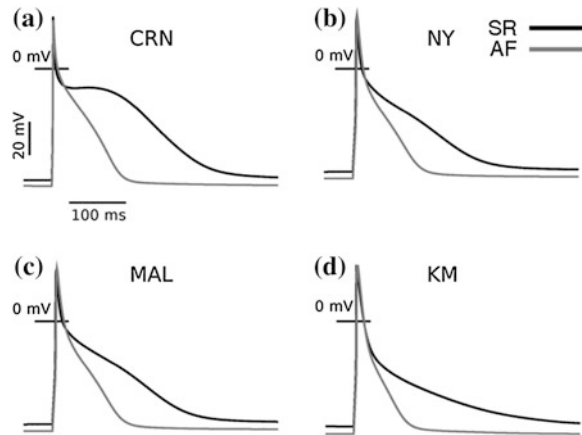


Fig. 2.22 Simulated effects of Af-induced ion channel remodelling in the four atrial models. Implementation of the Bosch model of remodelling associated with AF. Remodelled APs (grey) are shown compared to baseline APS (black). The scale bars in **a** apply to all four panels



2.10.5 AF-Induced Electrical Remodelling

A model of AF-induced remodelling, as incorporated by Zhang et al. (2005) [80] based upon the Bosch et al. 1999 clinical electrophysiological study [79], is incorporated into all four models (Fig. 2.22). It can be seen that in all four, remodelling results in a significantly shorter and more triangular shaped AP. It also reduces the RP by approximately 5 mV. The reduction on the APD_{90} of the CRN model is 61 %, NY model is 50 %, MAL model is 60 % and KM model is 74 %, compared to 60 % observed experimentally [79]. Hence, all models, with the exception of the KM model, behave well under remodelling conditions.

2.10.6 Comparison with Experimental Data

In Fig. 2.23, the four model APs are shown compared to a range of available APs from the human right atrial appendage (RAA) or unspecified right atrium (RA). They all fit within the large range observed, though it could be argued the spike and dome morphology of the CRN model is most commonly seen experimentally. Certainly, evidence suggests that this morphology is more common in APs measured in tissue, and the triangular morphology is more common in APs measured in single cell [86]. Similarly, Burashnikov et al. 2004 [87] indicate that APs from arterially-perfused tissue exhibit spike and dome morphologies, compared to superfused tissue which exhibit triangular morphologies. The APDs, upstroke velocities, amplitudes and RPs all lie within experimental ranges for all models.

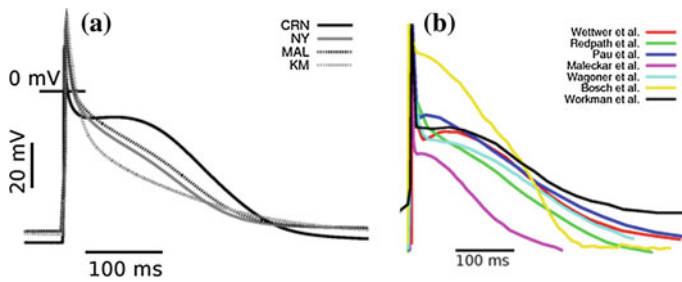


Fig. 2.23 Comparison with experimental data. Action potential traces from all four models (a) compared to a range of available experimental traces (b). Experimental traces taken from Wettwer et al. 2004 [81], Redpath et al. 2006 [82], Pau et al. 2007 [83], Maleckar et al. 2009 [69], Wagoner et al. [84], Bosch et al. [76] and Workman et al. [85]

2.10.7 Models for Regional Differences in the Atria

The suitability of the models as a base for a range of regional atrial cell models is assessed. This is done in a similar manner to that of Seemann et al. (2005) [65]. First, the four model APMs are compared to those of different regions within the canine atria (Fig. 2.24a). It is found that the CRN model shares most in common with the AP of the pectinate muscles (PM), whereas the NY, MAL and KM models share most in common with that of the atrioventricular ring (AVR). Then, the electrophysiological differences between these regions are incorporated into each model, and the morphology of the resulting AP is compared to that of the experimental trace. Details of the electrophysiological differences can be found in Seemann et al. (2005) [65]. The crista terminalis (CT) and AVR APs produced by the CRN model match well with the experimental traces (Fig. 2.24b-i). The PM AP produced by the NY and MAL models also matches well with the experimental traces, and could be argued to be closer to the real trace than the CRN model (Fig. 2.24b-ii, iii). However, the CT trace does not exhibit the definite and pronounced dome of the experimental trace, and the L-type calcium channel (I_{CaL}) needs to be increased by a much greater degree to produce this spike and dome morphology. Also, the difference in APD_{90} between the PM and AVR models is significantly smaller than is found experimentally and in the CRN versions. The KM model does not accurately reproduce the AP traces for the CT or PM, as increases in I_{CaL} (which primarily accounts for the differences) produce only very small differences in the APM. However, it is also the farthest morphologically from the AVR and hence it is likely that it is not accurate to consider it an AVR trace. There is also an intrinsic limitation to this technique in that morphology does not imply accurate electrophysiology for a particular region. Hence, whereas it may seem to resemble an AP from that region, it may be electrophysiologically distinct, and therefore applying changes assuming a base electrophysiology may be inaccurate.

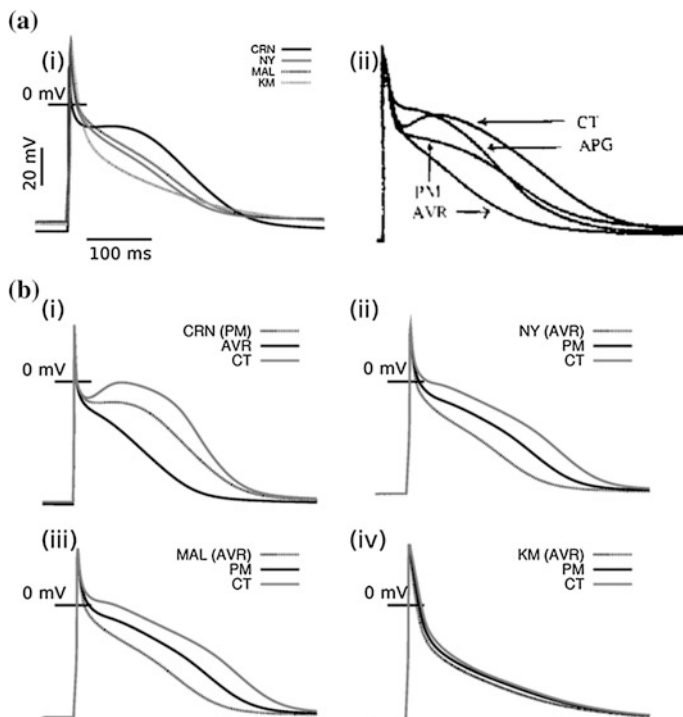


Fig. 2.24 Regional cell models. Regional cell models derived from each of the four human AP models. **a** APs from each of the four models (i) compared to canine experimental AP traces from Feng et al. 1998 [88] (ii). **b** Regional cell models, the *baseline* is shown in the *dotted line* in each panel. (i) CRN model, (ii) Nygren model, (iii) Maleckar model and (iv) KM model. The scale bars in **a** (i) apply to all panels in **b**

2.10.8 Conclusions

The four models exhibit different APM and restitution properties, and behave differently under remodelling and current modulation conditions. It is likely that the differing morphologies are due to data taken from different regions within the atria, but with the nature of the models this is difficult to state for certain. The CRN model is the only one of the four which exhibits a spike and dome morphology, which may be more representative of APs in the healthy atria. However, due to the large variety of APMs, even within the same region, this is also difficult to conclude, and all models are validated using experimental data and fit within experimental ranges for duration, peak and upstroke properties. The NY (and also derived MAL) model has issues with long term stability, something which the CRN model does not. However, the KM model solves this issue in the NY based models. The Ca^{2+} transient and dynamics observed experimentally are best modelled by the KM model. The CRN and MAL models behave best under

remodelling conditions, and the CRN model best replicates the range of regional cell APs observed. However, the formulations for I_{to} and I_{Kur} are outdated compared to the MAL model. The KM model is the least computationally efficient due to its complex intracellular structure.

References

1. Martini F (2006) Fundamentals of Anatomy & Physiology, 7th edn, Benjamin Cummings
2. Circulatory System <http://www.wikicell.org/eightSystemImage/circulatorySystem/Circulatory%20System/Circulatory%20System.jpg>
3. Diagram of the heart [Internet]. Available from: http://en.wikipedia.org/wiki/File:Diagram_of_the_human_heart_%28cropped%29.svg
4. Ho SY, McCarthy KP (2010) Anatomy of the left atrium for interventional electro physiologists. *Pacing Clin Electrophysiol* 33(5):620–627
5. Dobrzynski H, Li J, Tellez J, Greener ID, Nikolski VP, Wright SE et al (2005) Computer three-dimensional reconstruction of the sinoatrial node. *Circulation* 111(7):846–854
6. Chandler N, Aslanidi O, Buckley D, Inada S, Birchall S, Atkinson A et al (2011) Computer three-dimensional anatomical reconstruction of the human sinus node and a novel paranodal area. *Anat Rec (Hoboken)* 294(6):970–979
7. Schuessler RB, Boineau JP, Bromberg BI (1996) Origin of the sinus impulse. *J Cardiovasc Electrophysiol* 7(3):263–274
8. Boineau JP, Canavan TE, Schuessler RB, Cain ME, Corr PB, Cox JL (1988) Demonstration of a widely distributed atrial pacemaker complex in the human heart. *Circulation* 77(6):1221–1237
9. Boyett MR, Honjo H, Kodama I (2000) The sinoatrial node, a heterogeneous pacemaker structure. *Cardiovasc Res* 47(4):658–687
10. Boyett MR, Dobrzynski H, Lancaster MK, Jones SA, Honjo H, Kodama I (2003) Sophisticated architecture is required for the sinoatrial node to perform its normal pacemaker function. *J Cardiovasc Electrophysiol* 14(1):104–106
11. Boyett MR, Honjo H, Kodama I, Lancaster MK, Lei M, Musa H et al (2007) The sinoatrial node: cell size does matter. *Circ Res* 101(7):e81–e82
12. Li J, Greener ID, Inada S, Nikolski VP, Yamamoto M, Hancox JC et al (2008) Computer three-dimensional reconstruction of the atrioventricular node. *Circ Res* 102(8):975–985
13. Bonow RO (2011) Braunwald's heart disease: a textbook of cardiovascular medicine (2 Volume Set) (Heart Disease (Braunwald)), 9th edn. Elsevier Health Sciences
14. Stephenson RS, Boyett MR, Hart G, Nikolaidou T, Cai X, Corno AF et al (2012) Contrast enhanced micro-computed tomography resolves the 3-dimensional morphology of the cardiac conduction system in mammalian hearts. *PLoS ONE* 7(4):e35299
15. Electrical conduction system of the heart [Internet]. Wikipedia, the free encyclopedia (2012) [cited 2012 Sep 28]. Available from: http://en.wikipedia.org/w/index.php?title=Electrical_conduction_system_of_the_heart&oldid=513644044
16. Katz AM (2010) Physiology of the Heart, 5th Revised edn. Lippincott Williams and Wilkins
17. Ruiz M. http://en.wikipedia.org/wiki/File:Cell_membrane_detailed_diagram_4.svg
18. Hille B (2001) Ion Channels of Excitable Membranes. 3rd edn. Sinauer, Sunderland
19. Courtemanche M, Ramirez RJ, Nattel S (1998) Ionic mechanisms underlying human atrial action potential properties: insights from a mathematical model. *Am J Physiol* 275(1 Pt 2):H301–H321
20. Bers DM (2002) Cardiac excitation-contraction coupling. *Nature* 415(6868):198–205
21. Bers DM (2006) The beat goes on: diastolic noise that just won't quit. *Circ Res* 99(9): 921–923

22. DiFrancesco D (2010) The role of the funny current in pacemaker activity. *Circ Res* 106(3):434–446
23. Bogdanov KY, Maltsev VA, Vinogradova TM, Lyashkov AE, Spurgeon HA, Stern MD et al (2006) Membrane potential fluctuations resulting from submembrane Ca^{2+} releases in rabbit sinoatrial nodal cells impart an exponential phase to the late diastolic depolarization that controls their chronotropic state. *Circ Res* 99(9):979–987
24. DiFrancesco D, Ojeda C (1980) Properties of the current i_f in the sino-atrial node of the rabbit compared with those of the current i_K , in Purkinje fibres. *J Physiol* 308(1):353–367
25. Brown HF, DiFrancesco D, Noble SJ (1979) How does adrenaline accelerate the heart? *Nature* 280(5719):235–236
26. DiFrancesco D (1981) A new interpretation of the pace-maker current in calf Purkinje fibres. *J Physiol (Lond)* 314:359–376
27. DiFrancesco D (1981) A study of the ionic nature of the pace-maker current in calf Purkinje fibres. *J Physiol (Lond)* 314:377–393
28. Joung B, Chen P-S, Lin S-F (2011) The role of the calcium and the voltage clocks in sinoatrial node dysfunction. *Yonsei Med J* 52(2):211–219
29. Lakatta EG, DiFrancesco D (2009) What keeps us ticking: a funny current, a calcium clock, or both? *J Mol Cell Cardiol* 47(2):157–170
30. Zhang H, Holden AV, Noble D, Boyett MR (2002) Analysis of the chronotropic effect of acetylcholine on sinoatrial node cells. *J Cardiovasc Electrophysiol* 13(5):465–474
31. Gullberg GT, Defrise M, Panin VY, Zeng GL (2001) Efficient cardiac diffusion tensor MRI by three-dimensional reconstruction of solenoidal tensor fields. *Magn Reson Imaging* 19(2):233–256
32. Gilbert S, Bernus O, Holden A, Benson A (2009) A quantitative comparison of the myocardial fibre orientation in the rabbit as determined by histology and by diffusion tensor-MRI. In: Ayache N, Delingette H, Sermesant M (eds) *Functional imaging and modeling of the heart* [Internet]. Springer, Berlin/Heidelberg, pp 49–57. [cited 2012 Sep 16]. Available from: <http://www.springerlink.com/content/831534388x639506/abstract/>
33. Scollan DF, Holmes A, Winslow R, Forder J (1998) Histological validation of myocardial microstructure obtained from diffusion tensor magnetic resonance imaging. *Am J Physiol* 275(6 Pt 2):H2308–H2318
34. Fedorov VV, Ambrosi CM, Kostecki G, Hucker WJ, Glukhov AV, Wuskell JP et al (2011) Anatomic localization and autonomic modulation of atrioventricular junctional rhythm in failing human hearts. *Circ Arrhythm Electrophysiol* 4(4):515–525
35. Fedorov VV, Glukhov AV, Chang R, Kostecki G, Aferol H, Hucker WJ et al (2010) Optical mapping of the isolated coronary-perfused human sinus node. *J Am Coll Cardiol* 56(17):1386–1394
36. Kurian T, Ambrosi C, Hucker W, Fedorov VV, Efimov IR (2010) Anatomy and electrophysiology of the human AV node. *Pacing Clin Electrophysiol* 33(6):754–762
37. Laughner JJ, Ng FS, Sulkin MS, Arthur RM, Efimov IR (2012) Processing and analysis of cardiac optical mapping data obtained with potentiometric dyes. *Am j physiol. Heart and circulatory physiology* [Internet]. [cited 2012 Sep 22]; Available from: <http://www.ncbi.nlm.nih.gov/pubmed/22821993>
38. <http://en.wikipedia.org/wiki/File:SinusRhythmLabels.svg>
39. Lipman B, Casico T (1994) *ECG Assessment and Interpretation*. FA Davis Company, USA
40. Hampton JR (2008). *The ECG In Practice*. 5th ed. Churchill Livingstone
41. Conrath CE, Opthof T (2006) Ventricular repolarization: an overview of (patho)physiology, sympathetic effects and genetic aspects. *Prog Biophys Mol Biol* 92(3):269–307
42. Wikipedia contributors (2012) *Electrocardiography* [Internet]. Wikipedia, the free encyclopedia. Wikimedia Foundation, Inc. [cited 2012 Sep 16]. Available from: <http://en.wikipedia.org/w/index.php?title=Electrocardiography&oldid=512659345>
43. Fuster V, Rydén LE, Cannom DS, Crijns HJ, Curtis AB, Ellenbogen KA et al (2006) Guidelines for the management of patients with atrial fibrillation. Executive summary. *Rev Esp Cardiol* 59(12):1329

44. Wilson FN, Johnston FD, Macleod AG, Barker PS (1934) Electrocardiograms that represent the potential variations of a single electrode. *Am Heart J* 9(4):447–458
45. Goldberger E (1942) A simple, indifferent, electrocardiographic electrode of zero potential and a technique of obtaining augmented, unipolar, extremity leads. *Am Heart J* 23(4): 483–492
46. Coumel P (1994) Paroxysmal atrial fibrillation: a disorder of autonomic tone? *Eur Heart J* 15(Suppl A):9–16
47. Coumel P (1996) Autonomic influences in atrial tachyarrhythmias. *J Cardiovasc Electrophysiol* 7(10):999–1007
48. Levy MN (1988) Sympathetic-vagal interactions in the sinus and atrioventricular nodes. *Prog Clin Biol Res* 275:187–197
49. Kerin NZ, Louridas G, Edelstein J, Levy MN (1983) Interactions among the critical factors affecting sinus node function: the quantitative effects of the duration and frequency of atrial pacing and of vagal and sympathetic stimulation upon overdrive suppression of the sinus node. *Am Heart J* 105(2):215–223
50. Kuga K, Yamaguchi I, Sugishita Y, Ito I (1988) Assessment by autonomic blockade of age-related changes of the sinus node function and autonomic regulation in sick sinus syndrome. *Am J Cardiol* 61(4):361–366
51. Nattel S, Shiroshita-Takeshita A, Brundel BJM, Rivard L (2005) Mechanisms of atrial fibrillation: lessons from animal models. *Prog Cardiovasc Dis* 48(1):9–28
52. Benjamin EJ, Wolf PA, D'Agostino RB, Silbershatz H, Kannel WB, Levy D (1998) Impact of atrial fibrillation on the risk of death: the Framingham Heart Study. *Circulation* 98(10): 946–952
53. Anter E, Jessup M, Callans DJ (2009) Atrial fibrillation and heart failure: treatment considerations for a dual epidemic. *Circulation* 119(18):2516–2525
54. Baruscotti M, Bucchi A, Viscomi C, Mandelli G, Consalez G, Gneccchi-Rusconi T et al (2011) Deep bradycardia and heart block caused by inducible cardiac-specific knockout of the pacemaker channel gene *Hcn4*. *PNAS* 108(4):1705–1710
55. Butters TD, Aslanidi OV, Inada S, Boyett MR, Hancox JC, Lei M et al (2010) Mechanistic links between Na^+ channel (*SCN5A*) mutations and impaired cardiac pacemaking in sick sinus syndrome. *Circ Res* 107(1):126–137
56. Hodgkin AL, Huxley AF (1952) A quantitative description of membrane current and its application to conduction and excitation in nerve. *J Physiol (Lond)* 117(4):500–544
57. NOBLE D (1962) A modification of the Hodgkin–Huxley equations applicable to Purkinje fibre action and pace-maker potentials. *J Physiol (Lond)* 160:317–352
58. Levick J (1991) An introduction to cardiovascular physiology. Butterworth & Co Ltd
59. Decker KF, Heijman J, Silva JR, Hund TJ, Rudy Y (2009) Properties and ionic mechanisms of action potential adaptation, restitution, and accommodation in canine epicardium. *Am J Physiol Heart Circ Physiol* 296(4):H1017–H1026
60. Adeniran I, McPate MJ, Witchel HJ, Hancox JC, Zhang H (2011) Increased vulnerability of human ventricle to re-entrant excitation in hERG-linked variant 1 Short QT syndrome. *PLoS Comput Biol* 7(12):e1002313
61. Heijman J, Volders PGA, Westra RL, Rudy Y (2011) Local control of β -adrenergic stimulation: effects on ventricular myocyte electrophysiology and $\text{Ca}^{(2+)}$ -transient. *J Mol Cell Cardiol* 50(5):863–871
62. Clayton RH, Bernus O, Cherry EM, Dierckx H, Fenton FH, Mirabella L et al (2011) Models of cardiac tissue electrophysiology: progress, challenges and open questions. *Prog Biophys Mol Biol* 104(1–3):22–48
63. Rudy Y (2000) From genome to physiome: integrative models of cardiac excitation. *Ann Biomed Eng* 28(8):945–950
64. Aslanidi OV, Colman MA, Stott J, Dobrzynski H, Boyett MR, Holden AV et al (2011) 3D virtual human atria: a computational platform for studying clinical atrial fibrillation. *Prog Biophys Mol Biol* 107(1):156–168

65. Seemann G, Höper C, Sachse FB, Dössel O, Holden AV, Zhang H (2006) Heterogeneous three-dimensional anatomical and electrophysiological model of human atria. *Philos Transact A Math Phys Eng Sci* 364(1843):1465–1481
66. Moore JW, Ramon F (1974) On numerical integration of the Hodgkin and Huxley equations for a membrane action potential. *J Theor Biol* 45(1):249–273
67. Iserles A (1996) A first course in the numerical analysis of differential equations. Cambridge University Press, Cambridge
68. Nygren A, Fiset C, Firek L, Clark JW, Lindblad DS, Clark RB et al (1998) Mathematical model of an adult human atrial cell: the role of K^+ currents in repolarization. *Circ Res* 82(1):63–81
69. Maleckar MM, Greenstein JL, Giles WR, Trayanova NA (2009) K^+ current changes account for the rate dependence of the action potential in the human atrial myocyte. *Am J Physiol Heart Circ Physiol* 297(4):H1398–H1410
70. Gluais P, Bastide M, Grandmougin D, Fayad G, Adamantidis M (2004) Risperidone reduces K^+ currents in human atrial myocytes and prolongs repolarization in human myocardium. *Eur J Pharmacol* 497(2):215–222
71. Feng J, Xu D, Wang Z, Nattel S (1998) Ultrarapid delayed rectifier current inactivation in human atrial myocytes: properties and consequences. *Am J Physiol* 275(5 Pt 2):H1717–H1725
72. Koivumäki JT, Korhonen T, Tavi P (2011) Impact of sarcoplasmic reticulum calcium release on calcium dynamics and action potential morphology in human atrial myocytes: a computational study. *PLoS Comput Biol* 7(1):e1001067
73. Grandi E, Pandit SV, Voigt N, Workman AJ, Dobrev D, Jalife J et al (2011) Human atrial action potential and Ca^{2+} model: sinus rhythm and chronic atrial fibrillation. *Circ Res* 109(9):1055–1066
74. Cherry EM, Hastings HM, Evans SJ (2008) Dynamics of human atrial cell models: restitution, memory, and intracellular calcium dynamics in single cells. *Prog Biophys Mol Biol* 98(1):24–37
75. Cherry EM, Evans SJ (2008) Properties of two human atrial cell models in tissue: restitution, memory, propagation, and reentry. *J Theor Biol* 254(3):674–690
76. Llach A, Molina CE, Fernandes J, Padró J, Cinca J, Hove-Madsen L (2011) Sarcoplasmic reticulum and L-type Ca^{2+} channel activity regulate the beat-to-beat stability of calcium handling in human atrial myocytes. *J Physiol (Lond)* 589(Pt 13):3247–3262
77. Hatem SN, Bénardeau A, Rücker-Martin C, Marty I, De Chamisso P, Villaz M et al (1997) Different compartments of sarcoplasmic reticulum participate in the excitation-contraction coupling process in human atrial myocytes. *Circ Res* 80(3):345–353
78. Dobrev D, Wettwer E, Kortner A, Knaut M, Schüler S, Ravens U (2002) Human inward rectifier potassium channels in chronic and postoperative atrial fibrillation. *Cardiovasc Res* 54(2):397–404
79. Bosch RF, Zeng X, Grammer JB, Popovic K, Mewis C, Kühlkamp V (1999) Ionic mechanisms of electrical remodeling in human atrial fibrillation. *Cardiovasc Res* 44(1):121–131
80. Zhang H, Garratt CJ, Zhu J, Holden AV (2005) Role of up-regulation of IK_1 in action potential shortening associated with atrial fibrillation in humans. *Cardiovasc Res* 66(3):493–502
81. Wettwer E, Håla O, Christ T, Heubach JF, Dobrev D, Knaut M et al (2004) Role of IK_{Kur} in controlling action potential shape and contractility in the human atrium influence of chronic atrial fibrillation. *Circulation* 110(16):2299–2306
82. Redpath CJ, Rankin AC, Kane KA, Workman AJ (2006) Anti-adrenergic effects of endothelin on human atrial action potentials are potentially anti-arrhythmic. *J Mol Cell Cardiol* 40(5):717–724
83. Pau D, Workman AJ, Kane KA, Rankin AC (2007) Electrophysiological and arrhythmogenic effects of 5-hydroxytryptamine on human atrial cells are reduced in atrial fibrillation. *J Mol Cell Cardiol* 42(1):54–62

84. Van Wagoner DR, Pond AL, Lamorgese M, Rossie SS, McCarthy PM, Nerbonne JM (1999) Atrial L-type Ca^{2+} currents and human atrial fibrillation. *Circ Res* 85(5):428–436
85. Workman AJ, Pau D, Redpath CJ, Marshall GE, Russell JA, Norrie J et al (2009) Atrial cellular electrophysiological changes in patients with ventricular dysfunction may predispose to AF. *Heart Rhythm* 6(4):445–451
86. Koivumaki J, Christ T, Seemann G, Maleckar M (2012) Divergent action potential morphology in human atrial cells vs tissue: underlying ionic mechanisms. *Computing in cardiology, conference proceedings*
87. Burashnikov A, Mannava S, Antzelevitch C (2004) Transmembrane action potential heterogeneity in the canine isolated arterially perfused right atrium: effect of IKr and IKur/Ito block. *Am J Physiol Heart Circ Physiol* 286(6):H2393–H2400
88. Feng J, Yue L, Wang Z, Nattel S (1998) Ionic mechanisms of regional action potential heterogeneity in the canine right atrium. *Circ Res* 83(5):541–551

Mechanisms of Atrial Arrhythmias
Insights from the Development of a Biophysically
Detailed Model of the Human Atria

Colman, M.A.

2014, XXII, 256 p. 137 illus., 42 illus. in color., Hardcover

ISBN: 978-3-319-01642-9